PATTERN RECOGNITION IN EARTHQUAKE SWARMS FROM THE 2009 ERUPTION OF REDOUBT VOLCANO, ALASKA

by

Catherine Jeanne Carlisle

A thesis

submitted in partial fulfillment

of the requirements for the degree of

Master of Science in Geophysics

Boise State University

May 2013

BOISE STATE UNIVERSITY GRADUATE COLLEGE

DEFENSE COMMITTEE AND FINAL READING APPROVALS

of the thesis submitted by

Catherine Jeanne Carlisle

Thesis Title: Pattern Recognition in Earthquake Swarms from the 2009 Eruption of Redoubt Volcano, Alaska

Date of Final Oral Examination: 8 March 2013

The following individuals read and discussed the thesis submitted by student Catherine Jeanne Carlisle, and they evaluated her presentation and response to questions during the final oral examination. They found that the student passed the final oral examination.

Paul Michaels, Ph.D.	Chair, Supervisory Committee
Matt Haney, Ph.D.	Member, Supervisory Committee
Craig White, Ph.D.	Member, Supervisory Committee

The final reading approval of the thesis was granted by Paul Michaels, Ph.D., Chair of the Supervisory Committee. The thesis was approved for the Graduate College by John R. Pelton, Ph.D., Dean of the Graduate College.

ACKNOWLEDGMENT

There are many individuals and organizations that made this thesis possible. First and foremost, I would like to thank my advisor, Dr. Paul Michaels, for his support and teachings over the course of the last few years. I would also like to thank my other advising committee members, Dr. Matt Haney and Dr. Craig White, for their input along the way. Data was provided by Dr. Matt Haney at the Alaska Volcano Observatory and IRIS. Thank you to Boise State University Geoscience Department and the USGS for funding. Lastly, the constant support and encouragement from Brian, family, friends, and fellow geoscience students have made the last few years enjoyable. Thank you.

ABSTRACT

Earthquake swarms at volcanoes are common indicators of unrest and can be used to predict eruptions. However, not all earthquake swarms lead to an eruption but may die off instead. Variabilities in characteristics of swarms can lead to false predictions of an eruption. During the 2009 eruption of Redoubt Volcano in Alaska, there were five earthquake swarms, three of which preceded explosive eruptions and two that did not. These data were used to explore the variable characteristics that may be diagnostic of whether or not an eruption is imminent.

Data were recorded by the Alaska Volcano Observatory throughout the eruption. Band-pass filtering removed unwanted frequencies outside the long-period earthquake range of about 0.5-5.0 Hz. The onset of long-period earthquakes were cataloged and used to find features that varied between swarms. Duration times of individual events were calculated using the Arias Intensity. The power spectrum of the autocorrelation was used to determine central frequencies and shape factor values for each swarm. Earthquake swarms that preceded eruptions had short duration times. There was a small correlation between central frequency and shape factor values and eruption outcome and no correlation with time between earthquake swarm events.

TABLE OF CONTENTS

LIST OF TABLES

LIST OF FIGURES

CHAPTER 1:

INTRODUCTION

Seismicity at volcanoes is commonly an indicator of unrest and renewed volcanic activity. Seismic activity commonly precedes and accompanies eruptions and is an important tool in monitoring a volcano's eruptive state (Chouet *et al.*, 1994). However, just because seismicity occurs, doesn't mean an eruption is imminent (Moran *et al.*, 2011). Moran *et al.* (2011) explains that seismic phenomena have been associated with intrusions that have failed to erupt.

Volcanic eruptions can impact many people, such as those displaced because their homes are in danger or those dealing with canceled airline flights. The 1985 eruption of Nevado del Ruiz in Colombia triggered lahars that killed over 20,000 people in a nearby town (Witham, 2005). The 2010 eruption at Eyjafjallajokull in Iceland produced an ash cloud that disrupted air travel for almost a week (Mazzocchi *et al.*, 2010).

It is important to differentiate between when seismicity as a result of volcanic unrest leads to an explosive eruption and when it does not. Because earthquakes can occur before, during, and after an eruption, it is also important to be able to find differences in earthquakes to determine the stage of the eruption. By improving volcano monitoring techniques, scientists could potentially determine if and when an eruption might occur, more accurately predict the events during the eruption, and determine when the eruption might end. The goal of this research is to give a detailed look at varying characteristics of earthquake swarms to improve these volcano moni-

toring techniques. This study compares earthquake swarms that preceded eruptions and ones that died off during the 2009 eruption at Redoubt Volcano in Alaska with the goal of finding distinct differences between different types of earthquake swarms.

1.1 Volcano Monitoring

Attempts at volcano monitoring began at Mount Vesuvius with the building of an observatory in 1841. The goal of volcano monitoring is to determine what condition the volcano is in and assess what its future behavior might be. Not only is it important to determine when a volcano might erupt but also when the eruption is over. This is done with both field and lab methods, as described below.

There are many different methods and instruments used to monitor volcanoes. The most common approach is seismology. As magma moves through the crust, it can create vibrations in cracks, or fractures in rock as a result of new pressure. This can be picked up on seismometers long before the eruption begins. Francis and Oppenheimer (2004) explain that some of the most common seismology observations include the rate of earthquakes, the average earthquake amplitudes, the location of the hypocenters, and the type of event. These can all be indicators of when the eruption will occur or when it may be over.

An increase in the frequency of seismic events is the most common indicator that a volcano is ready for eruption. McNutt (2002) explains that the level of seismicity is usually directly related to the level of volcanic activity. More frequently occuring earthquakes means that the volcano is more likely to erupt.

Francis and Oppenheimer (2004) explain that another common approach to volcano monitoring is through geodesy, or measuring ground deformation. Ground de-

formation can result from the movement of magma or changes in pressure. Ground deformation is often recorded using GPS surveys, tiltmeters, strainmeters, and radar interferometry (Francis and Oppenheimer, 2004).

Changes in the SO_2 content of volcanic gases can be a common indicator of an imminent eruption, so it is important to monitor the geochemistry of surface gases. It is important to know the composition of the gas and the rate of emission. This can be done with physical sample collection, spectroscopic methods, and airborne ash measurements (Francis and Oppenheimer, 2004).

Francis and Oppenheimer (2004) explain there are many other geophysical methods that can be applied to volcano monitoring. One example is electromagnetic surveys since they detect changes in the permeability, pressure, and temperature of fluids such as magma. Gravimetric data may reveal the movement of magma since this also changes the location of mass below the crust, thus affecting the gravitational field. Microphones are often used to "listen" to the volcano and can record acoustic intensity variations. Thermal measurements reveal whether a volcano is heating up or cooling down using thermometers or infrared detectors. Seismology is one of the most robust methods, though, and the rest of this study will focus solely on seismic data.

1.2 Pattern Recognition

Pattern recognition is defined by Mulargia *et al.* (1991) generally as a search for structure in data. It can be applied to a large number of areas such as medicine and biology or stock market trends. More recently, scientists have begun to use pattern recognition to discriminate between different seismic signals at volcanoes.

Seismology is one of the most useful tools used in volcano monitoring and automatic pattern recognition algorithms reduce analyst workload when it comes to manually discriminating seismic signals. Novelo-Casanova and Valdes-Gonzalez (2008) used pattern recognition to discriminate between volcano-tectonic earthquakes and man-made signals, such as quarry blasts, at Popocatepetl Volcano in Mexico. The signal type was determined based on patterns in frequency spectrum and envelope shape. A similar study was completed by Scarpetta *et al.* (2005) at Mt. Vesuvius in Italy to discriminate between any volcanic seismic signal and other transient signals. Also, Mulargia *et al.* (1991) used pattern recognition algorithms to distinguish between different seismic signals common at volcanoes using Mt. Etna as an example.

Scientists have already established that seismic activity can be a precursor to volcanic eruptions and they have used pattern recognition to discriminate between the signals. However, not all seismic signals will lead to an eruption. The goal of this research is to find patterns to discriminate between earthquake swarms that lead to explosions and those that do not.

A similar study to this one was completed by Ketner and Power (in press), which looked at characteristics of seismic events that occurred during the 2009 eruption at Redoubt Volcano. Ketner and Power (in press) focused on a robust number of seismic events and characteristics, such as observations about event rate, duration, amplitude, and frequencies. The study looked at the same earthquake swarms as this study, plus a few more smaller swarms. In most cases, results were agreeable with this study, and they are explained in more detail in Chapter 4.

1.3 Volcanic Earthquakes

Before understanding patterns within earthquake swarms, it is important to understand the different types of earthquakes that occur at volcanoes and what they represent. The four main types of earthquakes at volcanoes are volcano-tectonic, hybrid, long-period, and tremor. These events vary in both source and signal, and each one can be an indicator of unrest. Examples of each earthquake waveform and frequency spectrum are shown in Figure 1.1.

1.3.1 Volcano-Tectonic Earthquakes

The largest magnitude earthquakes associated with volcanoes are volcano-tectonic (VT) earthquakes. Their waveform is similar to the earthquakes seen at tectonic boundaries, but they are generally not as large in magnitude. They can occur as a single earthquake or as a swarm of many earthquakes.

VT earthquakes result from shear failure within the volcano. According to Chouet (1996), VT seismicity is often an indication of renewed activity at a volcano. However, it is difficult to predict the time of eruption from VT earthquakes because they can occur days, months, and/or years before the actual eruption. These earthquakes are characterized by their relatively large magnitudes and high frequency spectrum. Their source may be from much deeper in the crust (up to 10 km) than other earthquakes associated with volcanoes (Lahr *et al.*, 1994), but can occur at shallow depths also. Because VT earthquakes originate from shear movement or rock failure, mixed first motions is one of their defining characteristics (Chouet, 1996). VT earthquakes have distinct P and S phases with peak frequencies between 6-8 Hz and significant energy up to 15 Hz (Power *et al.*, 1994); (Chouet, 1996).

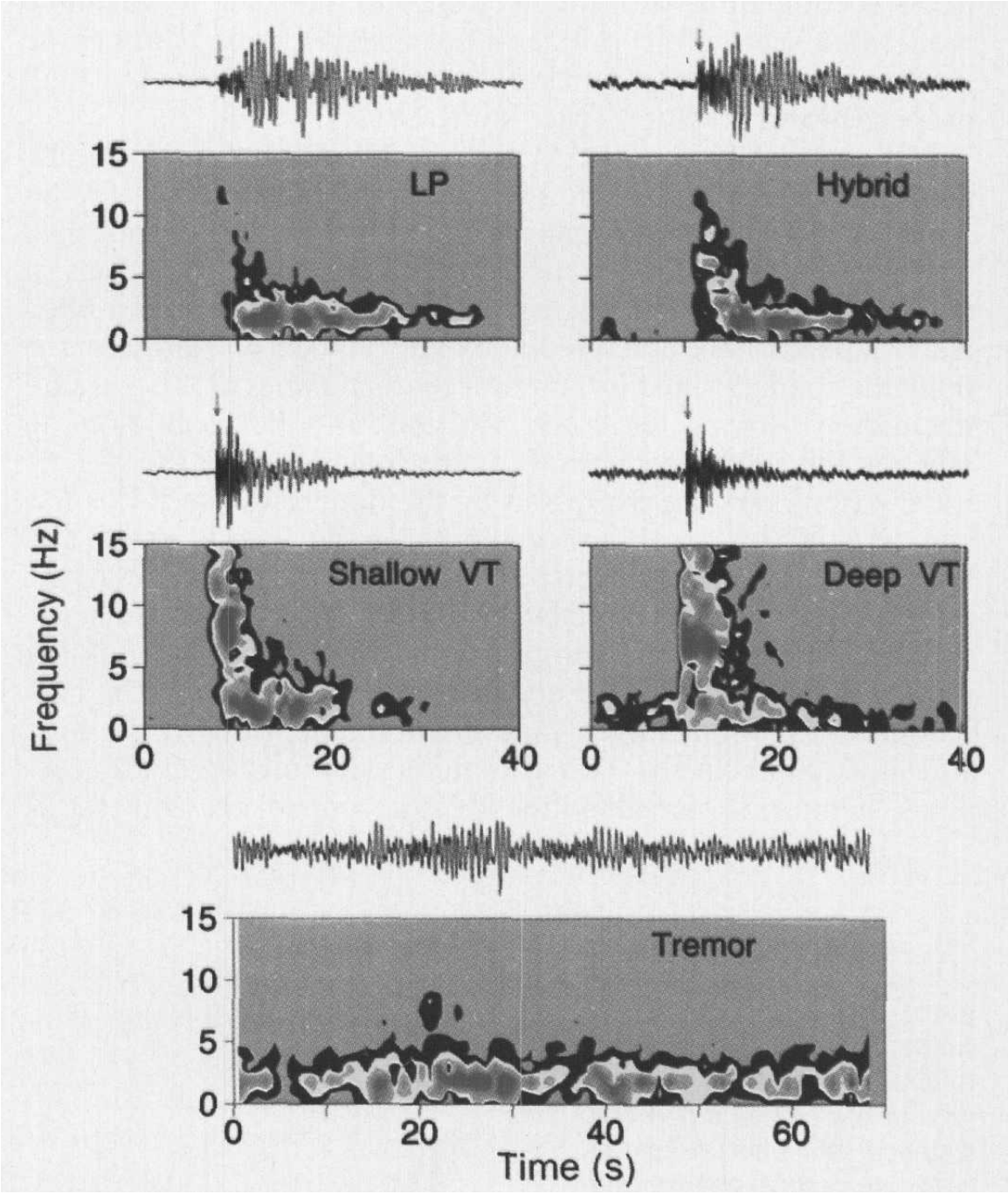

Figure 1.1: There are many types of earthquakes associated with volcanoes including volcano-tectonic, hybrid, long-period, and tremor (Chouet, 1996).

1.3.2 Long-Period Earthquakes

Another common type of earthquakes at volcanoes is long-period (LP), which is also known as b-type or low-frequency. They differ from VT earthquakes because they are the result of fluid and/or gas processes, which are not totally understood (McNutt, 2005). These earthquakes have peak frequencies near 1.5 Hz. Also, according to Chouet (1996), LP earthquakes that occur in swarms are very similar in their waveform signature. This can be interpreted as the repetitive excitation of a stationary source such as a crack connecting a magma reservoir and a hydrothermal reservoir (Chouet, 1996). As gas or fluid moves through the crack to equilibrate pressure, it creates LP earthquakes.

1.3.3 Hybrid Earthquakes

Hybrid Earthquakes are a mix between VT and LP earthquakes. Lahr *et al.* (1994) suggest hybrid events are caused by brittle failure occurring in fluid-filled areas, such as intersections of weak fractures and fluid-filled cracks. The waveforms of hybrid and LP events are similar in most characteristics, except for a more pronounced onset with mixed polarities and higher frequencies (Lahr *et al.*, 1994). The dominant frequency range for hybrid events is between 3-10 Hz (Neuberg *et al.*, 2000). Similar to VT and LP events, hybrid earthquakes commonly occur in earthquake swarms.

1.3.4 Tremor

According to Chouet *et al.* (1994), there is a strong link between tremor and LP earthquakes in both source and spectrum. The biggest difference is the duration of events. Tremor can be thought of as a continuous LP earthquake with a dominant

frequency near 1.5 Hertz (Chouet, 1996). Similarly to LP earthquakes, tremor is caused when magma flow encounters disturbances (Chouet, 1996).

1.3.5 Earthquake Swarms

Earthquakes associated with volcanic eruptions commonly occur in swarms. The swarms from the 2009 Redoubt eruption lasted anywhere from one hour to several days. They can be made up of VT, LP, or hybrid earthquakes, or sometimes a combination. McNutt (2005) explains that earthquakes occurring in swarms commonly have similar waveforms. This means that the source of the earthquakes is continuous and non-destructive (Chouet, 1996). The origin of these earthquakes is often near and beneath the site of the eruption (McNutt, 2005). Figure 1.2 shows volcano-tectonic earthquakes during the second swarm of the eruption.

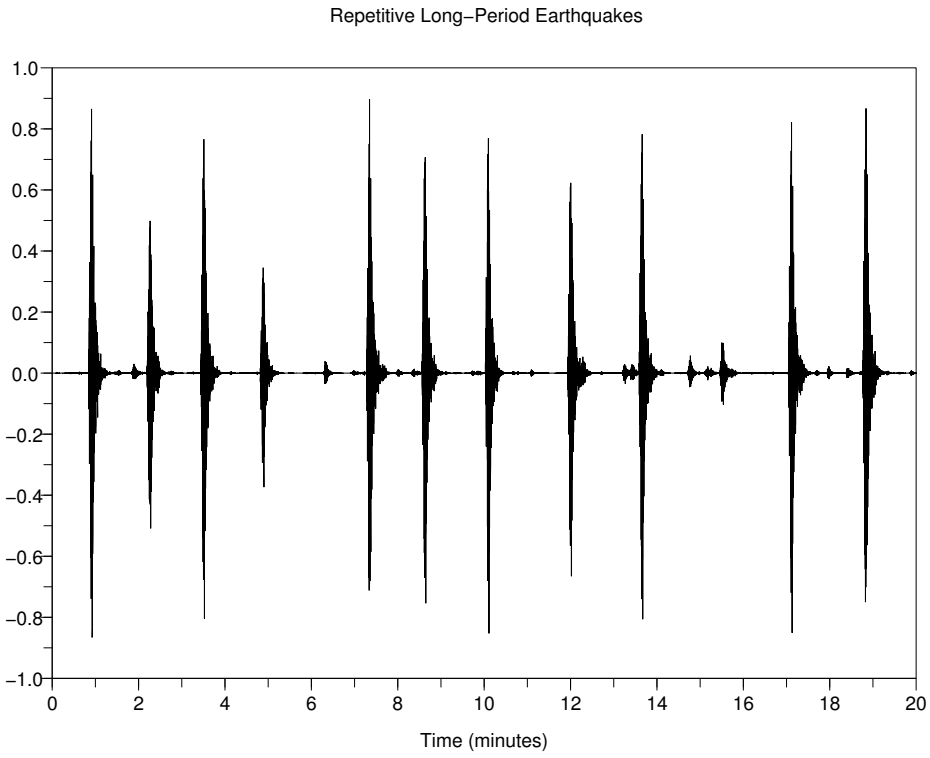

Figure 1.2: Volcanic earthquakes are commonly repetitive and found in swarms, such as these volcano-tectonic earthquakes. This shows over 12 earthquakes occurring in less than 20 minutes during the 8 hour swarm on 3/27/2009.

CHAPTER 2:
GEOLOGIC SETTING AND ERUPTION HISTORY

2.1 Introduction

Many years and geologic processes have made Redoubt Volcano into what it is today. This chapter provides the geologic history behind the Aleutian Arc volcanoes and Redoubt Volcano specifically, along with information about its eruption history and style.

2.2 Location

Redoubt Volcano is located 170 kilometers southwest of Anchorage and 80 kilometers west of the Kenai Peninsula. It is a strato-volcano with glacially dissected steep sides. Redoubt's peak reaches 3,110 meters above sea level and rises above the surrounding Chigmit Mountains (Till *et al.*, 1993).

Redoubt Volcano is one of over a hundred volcanoes that make up the Aleutian Volcanic Arc and is one of 41 historically active volcanoes along the arc; see Figure 2.1. As shown in Figure 2.1, Mount Spurr, Iliamna and Augustine neighbor Redoubt Volcano (Till *et al.*, 1993); (Bull *et al.*, 2012).

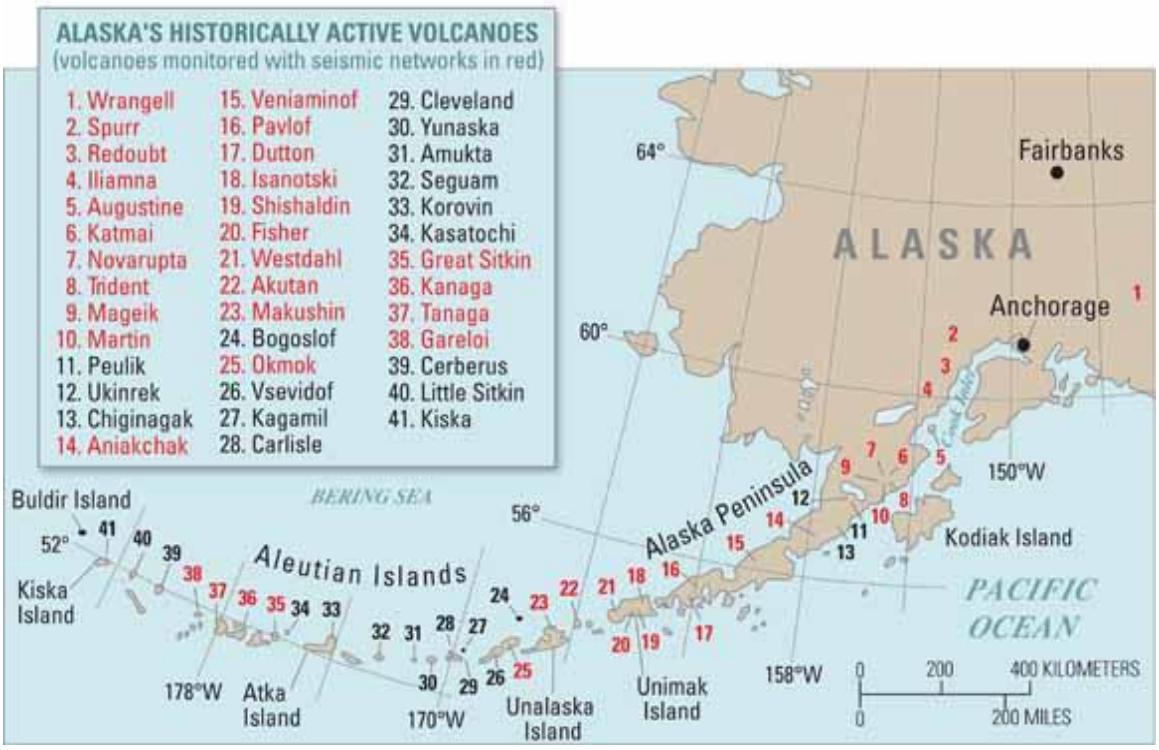

Figure 2.1: Volcanoes line the southern border of Alaska and make up a large portion of the ring of fire, which follows the edge of the Pacific Ocean, from usgs.gov.

2.3 Geologic Setting

In order to study Redoubt Volcano in detail, it is useful to understand its geologic setting and geologic history.

According to Vallier *et al.* (1994), the Aleutian arc is a volcanic mountain range along the northern rim of the Pacific Ocean Basin and stretches over 3,000 kilometers from the Kamchatka Peninsula, Russia to the Cook Inlet, Alaska. This volcanic arc is the result of the Pacific Plate converging and subducting under the North American plate. The volcanoes mostly parallel the subduction zone. The volcanoes that make up the Alaskan peninsula are some of the tallest, largest, and most explosive volcanoes that make up the Ring of Fire, the volcanic chain lining most borders of the Pacific Ocean (Miller and Richter, 1994).

The Aleutian Arc can be divided into two main sections, continental and oceanic (Fournelle *et al.*, 1994). Redoubt Volcano is located on the continental section, which spans from the western tip of the Alaskan Peninsula through the Cook Inlet. The continental section is bordered on the east by the Wrangell mountains (Fournelle *et al.*, 1994).

Miller and Richter (1994) explain the terrain that currently makes up the Alaskan Peninsula did not originate there. In fact, it may have formed far south, and in the early Cretaceous to early Tertiary it was accreted onto mainland Alaska.

Eastern Aleutian volcanoes lie on top of Jurassic to early Tertiary basement plutonic rocks and marine sedimentary rocks that formed between mid-Paleozoic to Holocene (Miller and Richter, 1994). Basement rocks are oldest to the east and become younger to the west.

The volcanoes along the Cook Inlet are quite similar. Potassium-Argon ages from

Redoubt and surrounding volcanoes show they began to form within the last million years (Miller and Richter, 1994). Most of the volcanoes along the Cook Inlet and Alaska Peninsula are stratocones and are made up of inter-layered lava flows and volcaniclastic rocks (Miller and Richter, 1994).

Miller and Richter (1994) explain some of the volcanic centers along the Alaska Peninsula are regularly spaced in segments, whereas others are spread out. Redoubt is isolated relative to other Peninsula and Inlet volcanoes. The largest spacing between centers is 94 kilometers, which is the distance between Mt. Spurr and Redoubt (Miller and Richter, 1994).

2.3.1 Geologic History of Redoubt Volcano

Till *et al.* (1993) explain that Redoubt Volcano's geologic history is made up of four distinct periods and began 400,000 years ago or more.

According to Till *et al.* (1993), the first period of volcanic activity at Redoubt was most likely the most explosive. It consisted of hot pyroclastic flows and shallow intrusions. The products from this period were also the most silicic in the volcano's history.

The second stage of Redoubt's history was the early-cone building period and occurred during the Pleistocene (Till *et al.*, 1993). This period produced the least silicic rocks. Its activity was characterized by many thin basalt and basaltic-andesite flows (Till *et al.*, 1993).

Till *et al.* (1993) continue to explain Redoubt's third stage was the late cone-building stage. This period produced thick, columnar andesite flows that make up the upper edifice of the Redoubt. The flows range in thickness of 30 to 60 meters

(Till *et al.*, 1993).

The last and current period of activity at Redoubt makes up the last 100,000 years or so. Till *et al.* (1993) explain the deposits from this stage are mainly from debris flows and widespread tephra falls. These deposits are mainly andesitic in composition, similar to the previous period of activity.

McNutt (1996) explains that one of the best ways to assess characteristics of volcanic eruptions is by looking at the past eruptive activity. The surrounding geology and eruptive history give many clues to the type of eruption style. For example, volcanoes that erupt silicic materials tend to be more explosive and are from a central vent, whereas basaltic eruptions are typically on the flank of the volcano and more effusive (McNutt, 1996). Because Redoubt tends to erupt andesitic material, it is safe to assume that its eruptions are more explosive and are from a central vent. Seismology can be used to identify more features that are specific to these types of eruptions.

2.4 Eruption Style

Redoubt Volcano has erupted over 50 times in the last 10,000 years and at least five times since 1700. Its eruptions tend to be explosive and accompanied by lahars, ash plumes, and lava domes (Bull *et al.*, 2012). The most recent eruptions are described below.

2.4.1 1989-1990 Eruption

A major eruption at Redoubt Volcano occurred from December 14, 1989 - April 31, 1990. Just as with the 2009 eruption, many earthquake swarms preceded and accompanied the eruption. Long-period swarms preceded 14 of the 22 explosions that made up the eruption (Chouet, 1996). Miller and Richter (1994) explain that unrest began in September, 1989 with mild seismicity. The first swarm began on December 13, 1989 and increased in intensity before turning into high-amplitude tremor and preceding the initial explosion on December 14 (Power *et al.*, 1994). Most of the tephra eruptions followed phases of dome-building and LP earthquake swarms. No swarms occurred after the last dome collapse on April 29, 1990 (Power *et al.*, 1994). Power *et al.* (1994) found the hypocenters of the LP earthquakes ranged from 0-3 kilometers directly below the volcano's summit.

2.4.2 2009 Eruption

The 2009 eruption at Redoubt Volcano began explosively on March 23, 2009. However, volcanic unrest began as early as May, 2008 (Bull *et al.*, 2012). Bull *et al.* (2012) divided the eruption into 3 main phases, including the precursory phase (July 2008-March 2009), the explosive phase (March 15-April 4, 2009), and the effusive phase (April 4-July 1, 2009).

The precursory phase began when field geologists noticed a hydrogen sulfide odor coming from Redoubt (Bull and Buurman, in press). Other evidence of unrest included explosion-like noises reported by residents living near Redoubt and a volcanic tremor signal in September (Bull and Buurman, in press). Towards the end of 2008, H_2S, SO_2, and CO_2 gas levels increased, rock became more exposed surrounding

fumeroles, and deep long-period earthquakes began below the edifice (Bull and Buurman, in press); (Power *et al.*, in press). Seismicity increased in late January with bursts of tremor and again in late February when a volcano-tectonic earthquake swarm lasted 31 hours (Bull and Buurman, in press). Also in late February, a tremor signal began and sustained for 20 days, and glacial melting occured as a result of increased heat flux (Bull and Buurman, in press).

Bull and Buurman (in press) describe the chronology of the explosions that made up the eruption as follows. The explosive phase began on March 15 with a phreatic explosion and was followed by seismic activity including tremor and a 60-hour earthquake swarm that began on March 20. The first magmatic explosion occurred on March 23 and was followed by eight other explosions before the end of March 24. Following the first nine explosions was a 60-hour pause in activity and then two more explosions on March 26 occurring less than an hour apart. Over ten explosions occurred after another half day of quiescence, which included an eight-hour earthquake swarm. There was another earthquake swarm on March 29 that lasted one hour, however, there was not a proceeding explosion. The last event of the phase, consisting of three small explosions, occurred on April 4-5 following another earthquake swarm.

Bull and Buurman (in press) describe the last phase of the eruption as the effusive phase, which began after the explosions on April 4 and 5. During this time, the last lava dome was built and remained since there were not any more dome-destroying events. There was an earthquake swarm that occurred during the effusive phase in the beginning of May. It was the longest swarm but did not result in an explosion as some of the other swarms did. By July 1, 2009, changes in dome volume stopped and seismicity returned to background levels. Thus, the eruption was over.

2.4.3 Earthquake Swarms Associated with 2009 Eruption

There were five long-period earthquake swarms associated with the 2009 eruption at Redoubt Volcano. Three of the swarms preceded volcanic explosions while the other two died off. These swarms had different types of earthquakes and eruption outcomes.

The first swarm (S1) began on March 22 at 2:14 am according to Thompson and West (2010) and lasted until March 23 at 6:13 am. The swarm consisted of repetitive similar hybrid earthquakes. Ketner and Power (in press) explain that S1 is made up of many families of earthquakes, more so than any other swarm, and could represent different active sources. A waveform example is shown in Figure 2.2. The outcome of S1 was the first magmatic explosion of the eruption.

The second swarm (S2) began at the beginning of March 27 (0:00 hours) and lasted until about 08:00 hours. Just like the previous earthquake swarm, it also ended with a magmatic explosion. There is some debate as to the type of earthquakes that make up S2. They are not defined by a single type of volcanic earthquake. The most accepted theory is that the swarm is made up of VT earthquakes (Hotovec *et al.*, in press). S2 earthquakes had the largest magnitudes out of any of the swarms. Characteristic of VT earthquakes, they are higher in peak frequency and have visible P and S waves on some stations. However, similar to LP earthquakes, events have similar waveforms and polarity. Figure 2.3 show two different waveforms of the same earthquake from different stations. The top waveform, from RD03, appears LP whereas the bottom waveform, from RD01, has VT characteristics. Because of the clear signal on RD01, they are considered VT. More information on instruments and data acquisition can be found in Chapter 3.

Unlike the first two swarms, the third (S3) did not precede an explosion. S3 was

the shortest of all the earthquake swarms. It began at 07:50 on March 29 and lasted just over an hour ending at 09:00. S3 earthquakes, shown in Figure 2.4, can best be described as hybrid. On station RD01, there are clear P and S waves, but peak frequencies are under 5 Hz.

The last swarm that preceded an explosion (S4) began on April 2 at 16:23 and lasted until 13:57 on April 4, which is when the explosion commenced. The April 4 explosion was the last of the eruption. S4 is made up LP earthquakes, defined by their lack of clear P and S wave arrivals and low frequency spectrum. An example waveform from the swarm is shown in Figure 2.4.

The last swarm of the eruption (S5) occurred during the effusive phase and began gradually on May 2 around 17:00. It was by far the longest of the earthquake swarms since it lasted until May 10. Similar to S3, this swarm did not end with a magmatic explosion but a small ashy emission instead. S5 is made up of LP earthquakes, as shown in the waveform in Figure 2.6.

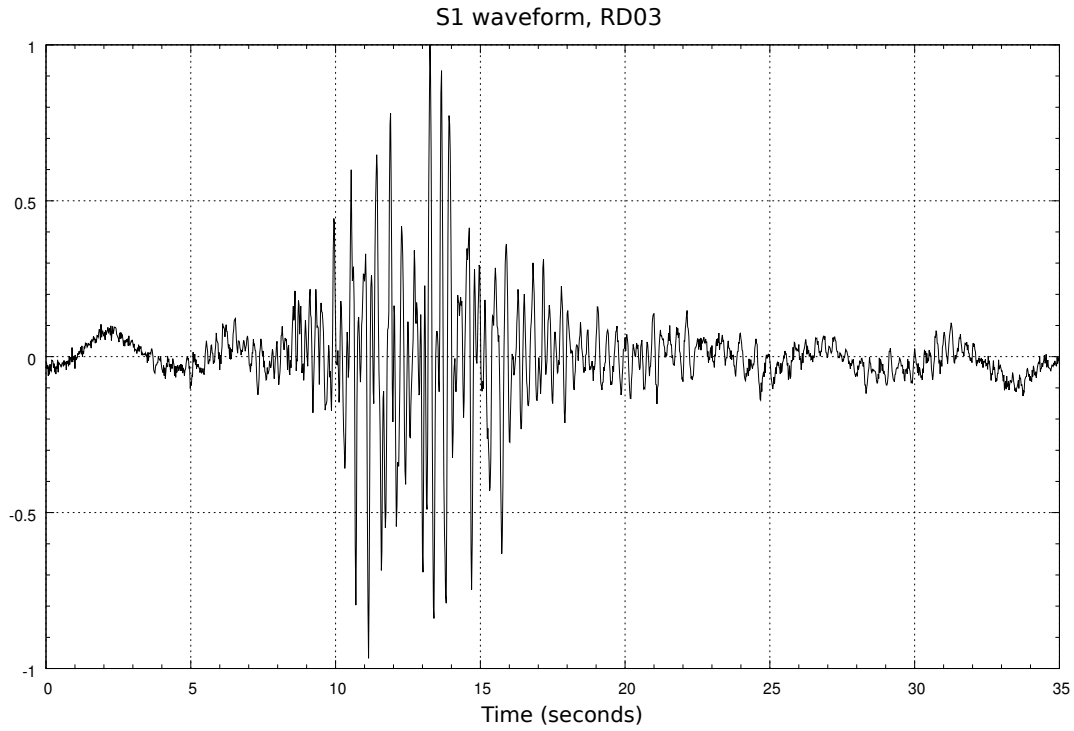

Figure 2.2: The first swarm of the eruption (S1) consisted of many hybrid earthquakes lasting from 3/22/09-3/23/2009 and preceded the first explosion.

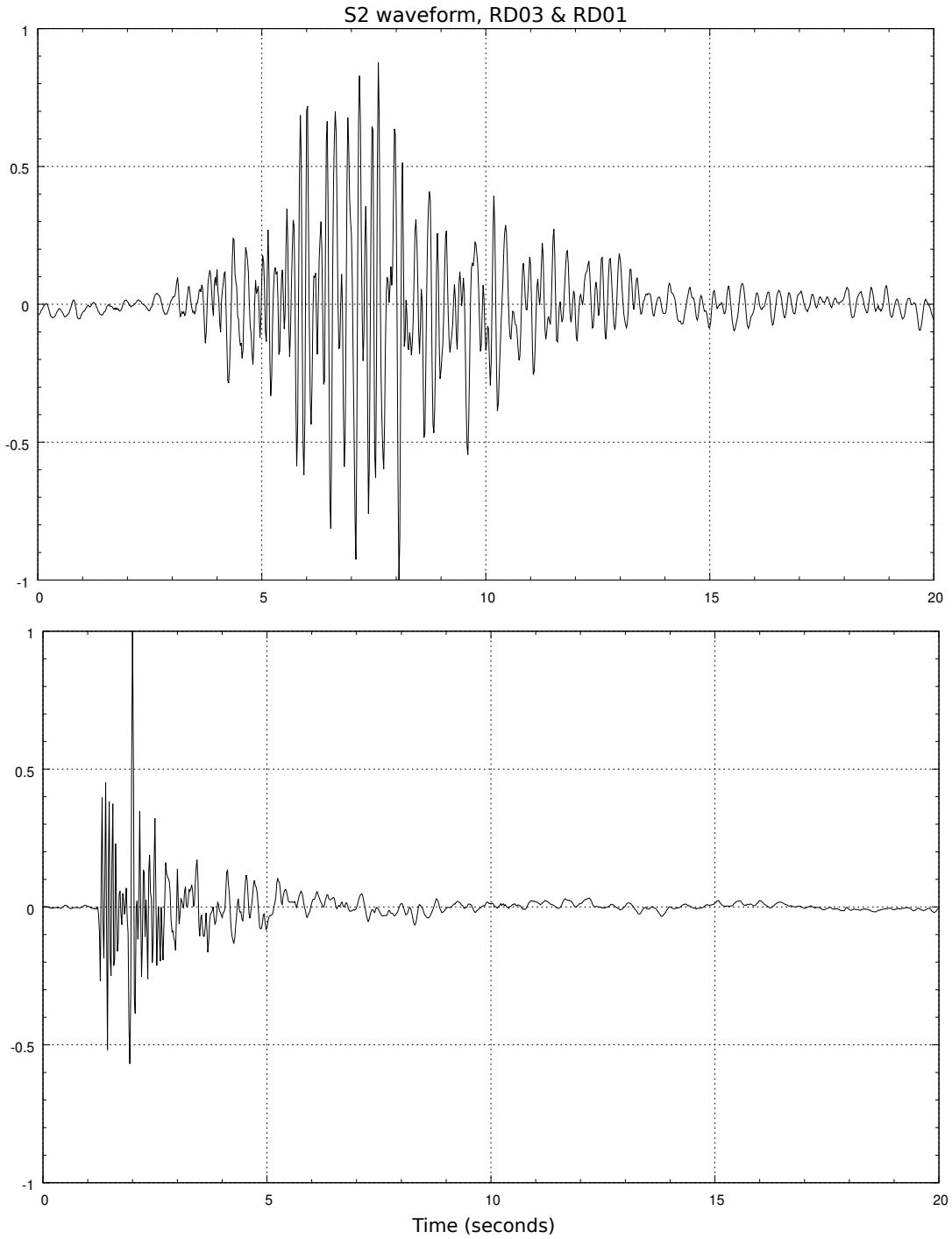

Figure 2.3: Two waveforms of the same earthquake on different stations, RD03 (top) and RD01 (bottom), show both LP and VT characteristics. Both waveforms are from unfiltered data. S2 lasted about 8 hours and preceded an explosion.

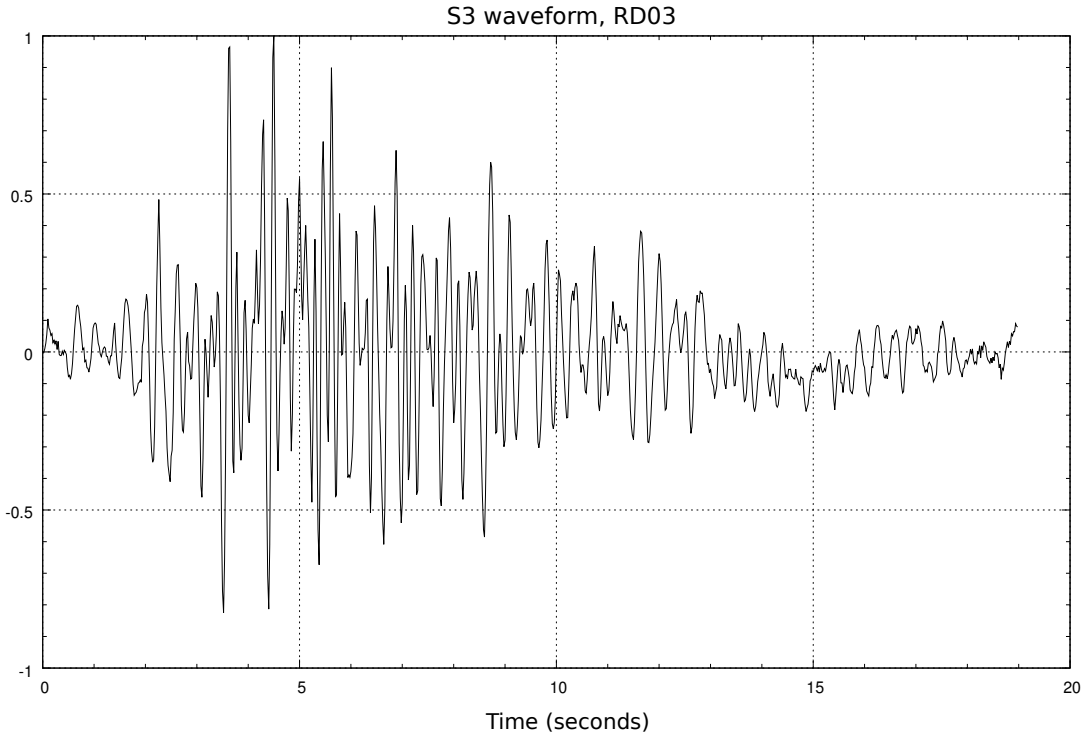

Figure 2.4: S3 was the shortest swarm lasting just over an hour, and it did not precede an explosion. The events are best described as hybrid events.

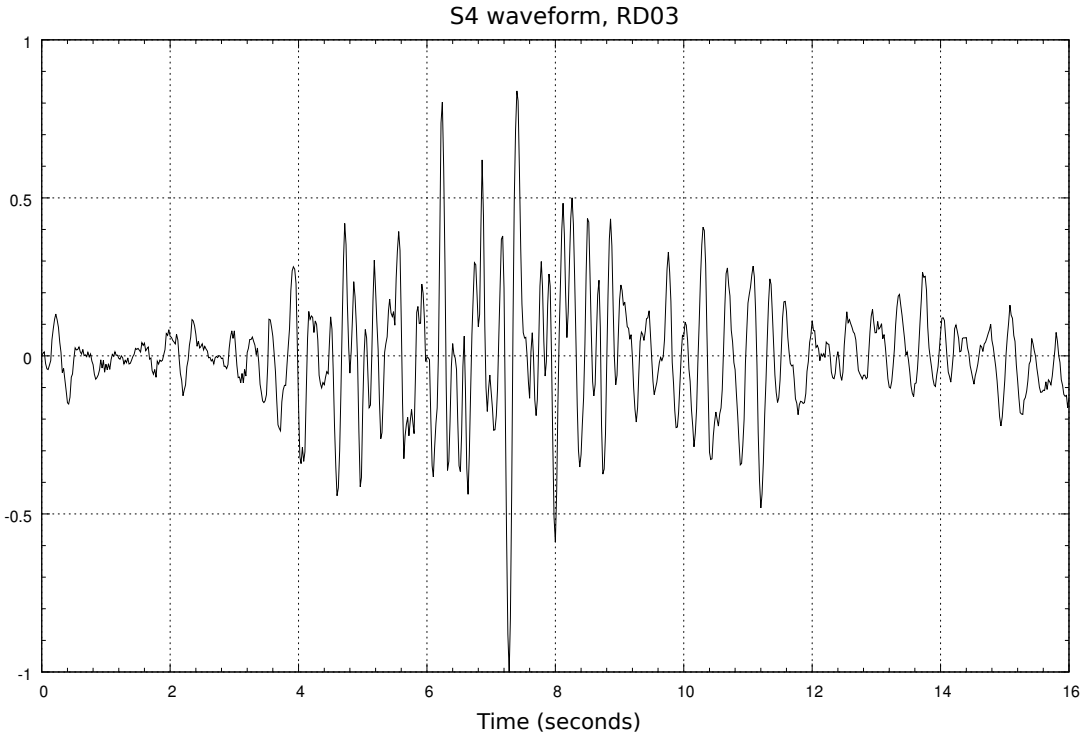

Figure 2.5: S4 preceded the largest and last explosions of the entire eruption. The events are best described as long-period events.

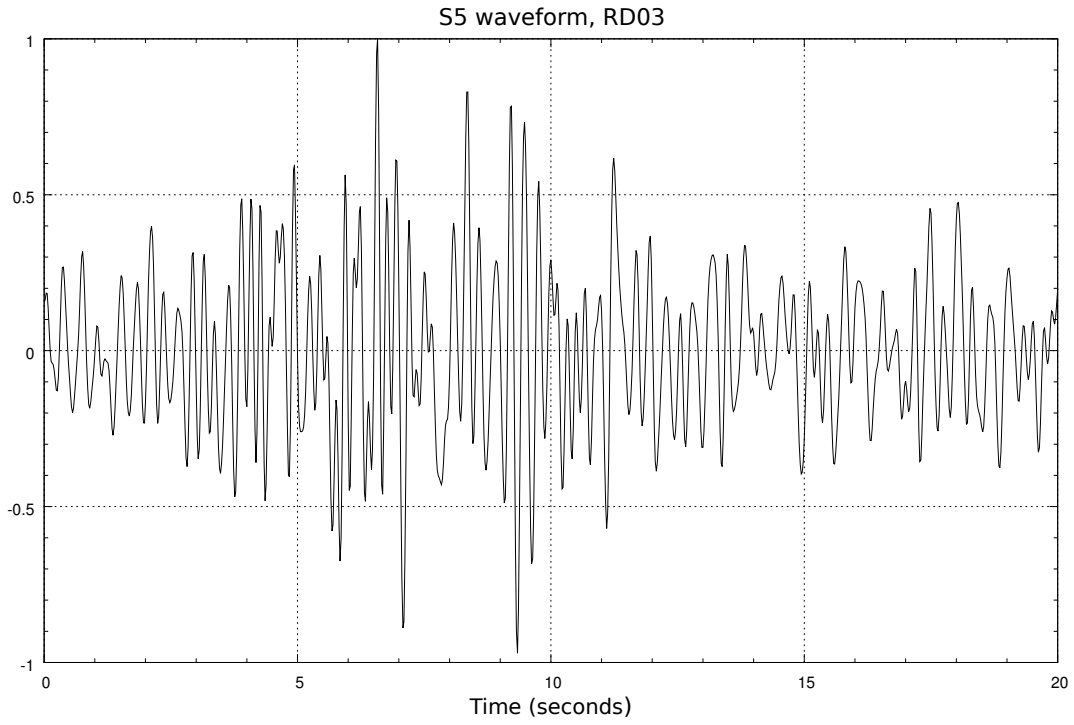

Figure 2.6: S5 was the long swarm lasting from 5/2/09-5/10/09. It is made up of LP earthquakes, defined by their low frequency spectrum and lack of clear P and S waves.

CHAPTER 3:

SIGNAL PROCESSING

In this work, several methods were used to search for patterns within earthquake swarms, most of which were focused on digital signal processing. This chapter explains the methods used in detail, starting with data acquisition. Other topics include new approaches to data filtering and automatic earthquake picking along with the patterns explored.

3.1 Data Acquisition

The Alaska Volcano Observatory has a large network of seismometers used to seismically monitor active volcanoes in Alaska. Redoubt Volcano has seven permanent seismometers. When Redoubt began showing signs of unrest, other broadband seismometers were deployed. Table 3.1 shows details about the instruments that recorded seismic data during the eruption and Figure 3.1 shows the station locations relative to Redoubt's summit.

Seismic data were acquired from IRIS seismiquery database and from personal communication with Dr. Matt Haney. Because the point of this research was to locate patterns within earthquake swarms, it is important to control as many variables as possible. For this reason, the data used in signal processing were the data collected on RD03. This removes signal uncertainty as a result of geology and path interference. Data collected on RD03 showed the least amount of noise and a lack of breaks in

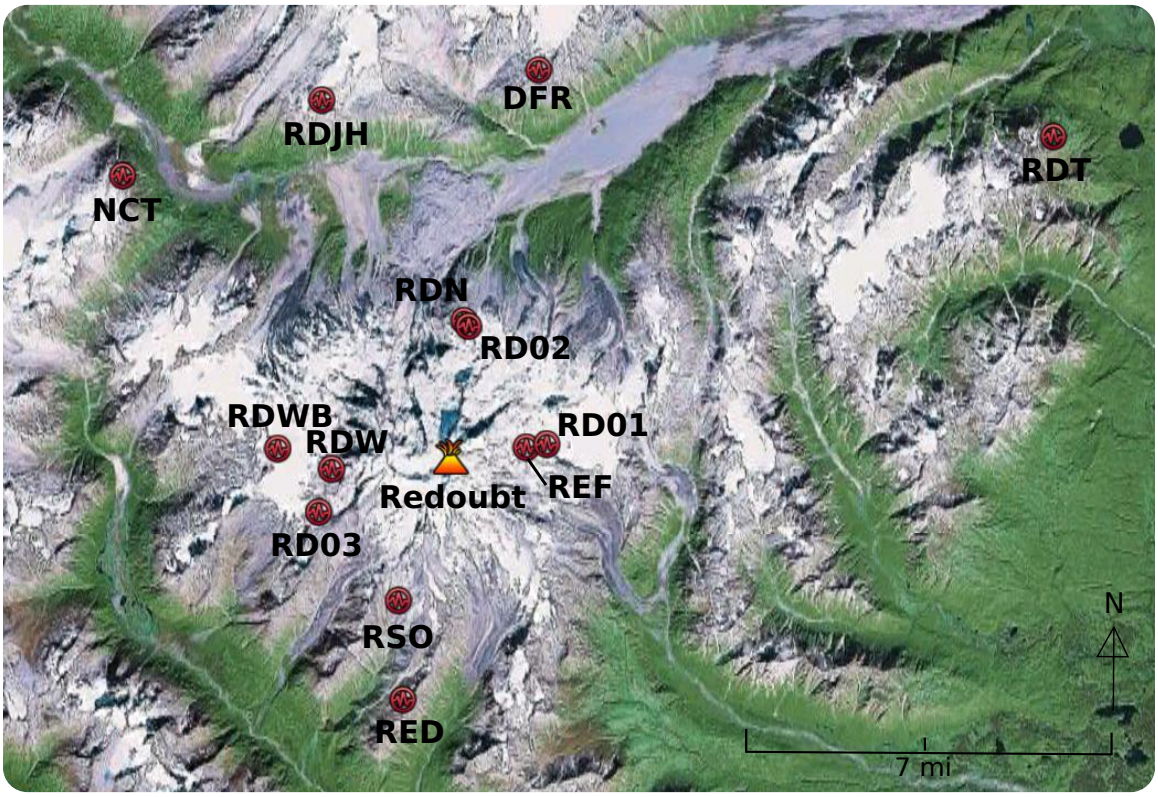

Figure 3.1: Thirteen seismometers recorded data for all or portions of the 2009 eruption at Redoubt. Most of the data used came from RD03, located southwest of the summit. Data were recorded by the Alaska Volcano Observatory. Figure was modified from Google Earth.

Station Name	Dates of Operation	Instrument	Components
RDN	11/01/2005-present	Mark L-4 1 Hz	Z
NCT	11/01/2005-present	Mark L-4 1 Hz	Z
DFR	11/01/2005-present	Mark L-4 1 Hz	Z
RDT	11/01/2005-present	Mark L-4 1 Hz	Z
RSO	11/01/2005-3/24/2009, 4-16/2009-present	Mark L-4 1 Hz	Z
REF	11/01/2005-present	L22D	E,N,Z
RED	11/01/2005-present	L22D	E,N,Z
RDWB	02/24/2009-present	CMG-6TD-T6054	E,N,Z
RDJH	02/04/2009-present	CMG-6TD-T6054	E,N,Z
RDW	03/22/2009-06/07/2009	CMG-6TD-T6054	E,N,Z
RD01	03/22/2009-06/07/2009	CMG-6TD-T6054	E,N,Z
RD02	03/22/2009-06/07/2009	CMG-6TD-T6054	E,N,Z
RD03	03/22/2009-06/07/2009	CMG-6TD-T6054	E,N,Z

Table 3.1: Thirteen stations collected seismic data during the Redoubt eruption. These stations are listed above along with the dates they were in operation, the instrument type, and the components.

data for the entire period of interest. Unless otherwise stated, it can be assumed that processing was on data solely from RD03. The main exception was the use of data from RD01 to help distinguish the types of earthquakes that made up each swarm, as described in the previous chapter.

Data were received in the form of SAC files from Dr. Haney and SEED files from IRIS. The SEED files were converted to SAC using rdseed. For simpler processing, SAC files were then converted to ascii or txt files using readsac2, a program by Dr. Paul Michaels. Processing was done mainly using Scilab.

3.2 Data Processing

Before searching for patterns within data, the data had to be filtered and earthquake arrivals were automatically picked. After routine signal processing, different features were explored.

3.2.1 Audacity Noise Removal

A lot of seismic signals begin with background noise. This can hide the signal of interest and make processing difficult. The Noise Removal function in Audacity can be used to removed unwanted noise. Audacity is an open-source signal processing program designed for audio processing but can be used on any digital signal.

The first step in noise removal using audacity is to convert ascii files to wav files. This is done with the wavwrite command in Scilab after the data are normalized and transposed to a row vector.

Once the data are opened in Audacity, the noise between events can be removed. A small portion of the noisy data is selected as the Noise Profile. Then, the entire signal is selected and the Noise Removal options allows for the removal of the noise profile from the entire signal. The new reduced-noise signal can be exported from Audacity as a wav file. The wavread command in Scilab reads in the file, which can then be converted back to ascii for more processing. Figure 3.2 shows a small window from swarm S2 prior to any other filtering and the effect Audacity Noise Removal has on the signal. Because the noise isn't completely removed, band-pass filtering would be the next logical step.

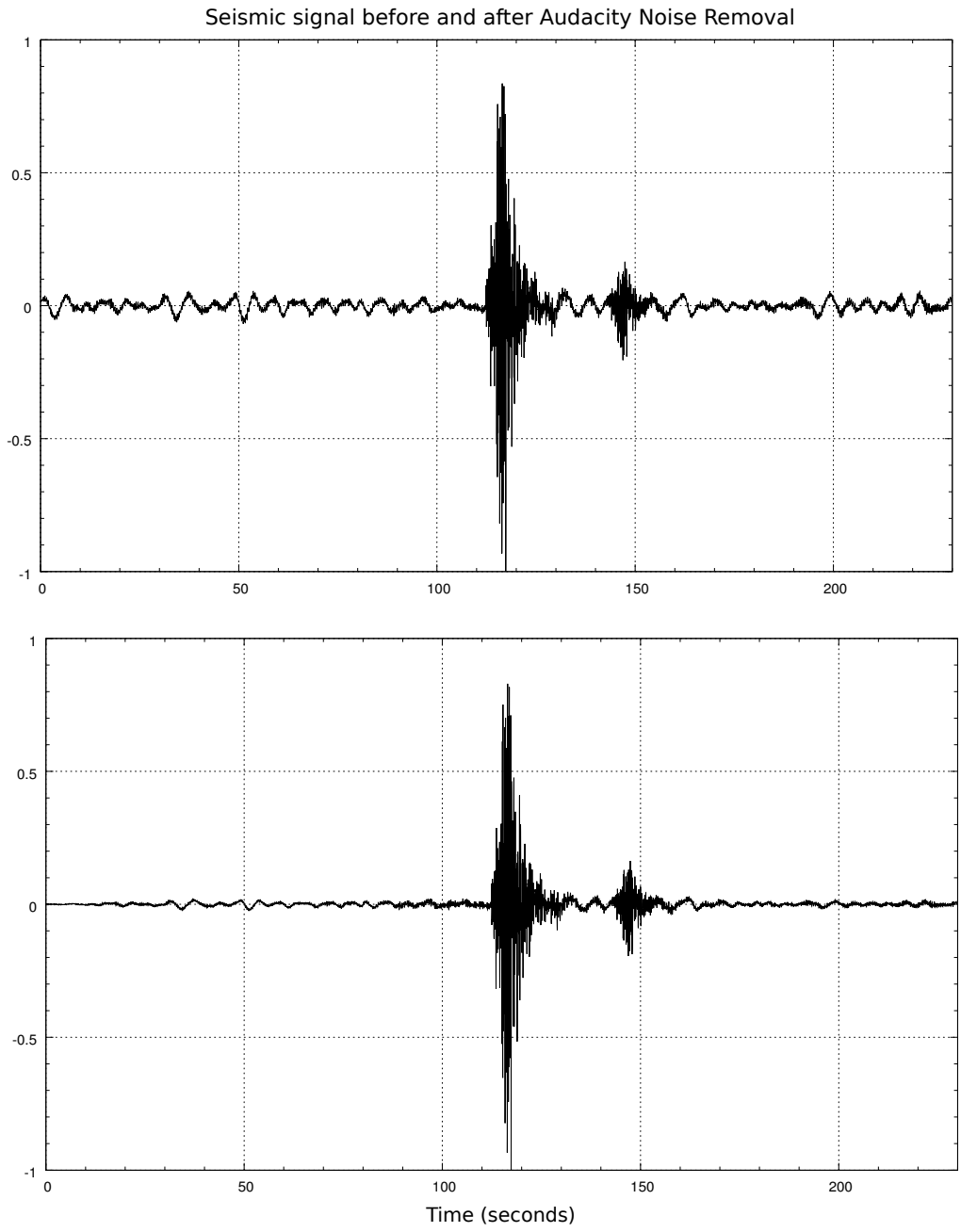

Figure 3.2: Audacity Noise Removal can be used to remove some noise from seismic signals.

3.2.2 Band Pass Filtering

Some of the data have a very strong low frequency signal. Earthquakes are overprinted onto this noise, which makes data processing such as automatic event picking difficult. By applying a band-pass filter, high and low frequencies are removed from the signal and should make further data processing possible and more accurate.

Most of the data acquired during the 2009 eruption contains a strong low-frequency signal ranging from 0-0.5 Hertz and is most likely a result of ocean microseisms. According to Schulte-Pelkum *et al.* (2004), ocean microseisms typically occur in two different frequency ranges of 0.07-0.10 Hz and 0.14-0.20 Hz. Ocean microseisms are defined by Schulte-Pelkum *et al.* (2004) as continuous seismic signals caused by the interaction of ocean swells with each other and with land. The first frequency band of 0.07-0.10 Hz may be as a result of ocean swells interacting with a shallow sea floor. The second frequency band (0.14-0.20 Hz), the more dominant band for ocean microseisms, is the result of the interaction of two opposing wavefields (Schulte-Pelkum *et al.*, 2004). Figure 3.3 shows three long-period earthquakes with a strong background noise created by ocean microseisms and the corresponding frequency spectrum.

The first step in band-pass filtering is to determine which frequencies need to be removed. This can be done by taking a fast fourier transform of an event and observing the range of strong low frequencies. Figure 3.3 shows the signal has a very strong low-frequency signal. The cut-off frequency for the band-pass filter based on Figure 3.3 is 0.5 Hz on the low end and 5.0 Hz on the high end.

The next step in noise removal is to read in data and specify the sampling interval, filter order, and the cut-off frequency. The options chosen for the filter function in

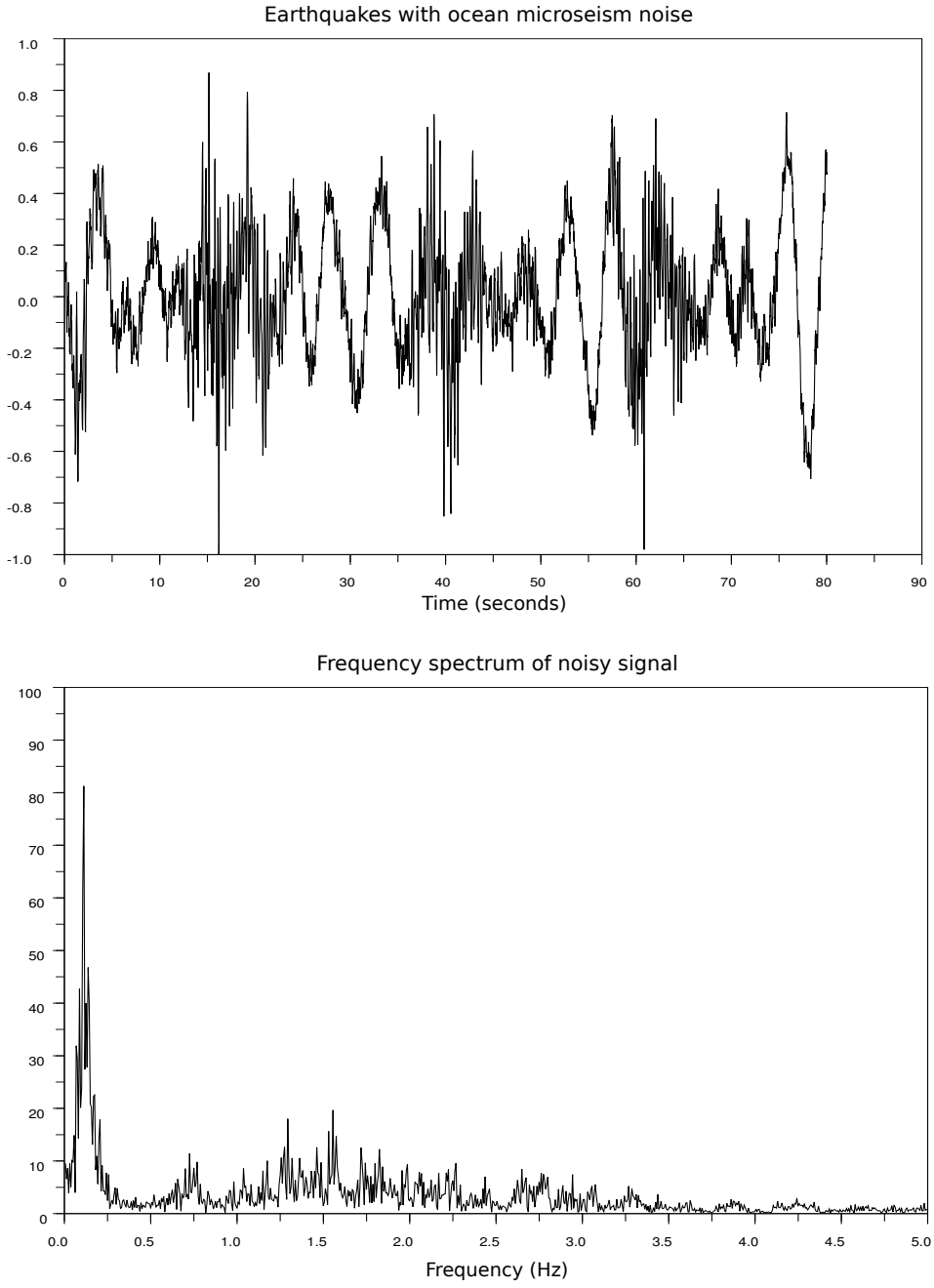

Figure 3.3: A common source of seismic noise is from ocean microseisms, which can be a result of the interaction of two wavefields or a wave with a shallow ocean bottom. This figure shows three long-period earthquakes with strong low-frequency noise as a result of the microseisms and its corresponding frequency spectrum.

Scilab are band-pass and Butterworth. Unwanted frequencies are thus removed, which allows for further data processing. Figure 3.4 shows the seismic signal and corresponding frequency spectrum with reduced noise after band-pass filtering is complete.

3.2.3 Automatic Earthquake Picking

An automatic earthquake picking algorithm is essential to speeding up data processing. An alternative approach is based on a forward/backward energy ratio of the amplitude of the signal.

The first and most common method of automatic earthquake picking is the short-term average/long-term average method. Rex Allen introduced this method in 1978 in hopes of creating a computer program that could duplicate the work of an analyst in detecting the arrival of earthquakes. Allen (1978) wanted to be sure the algorithm could distinguish earthquakes from other noise and to do so in real time. The algorithm is based on Equation 3.1, where $f(t)$ is the time series, $f'(t)$ is the first difference, and C_2 is a weighted constant.

$$E(t) = f(t)^2 + C_2 + f'(t)^2 \tag{3.1}$$

According to Allen (1978), the algorithm uses a short-term average and a long-term average of the quantity $E(t)$. If the short-term average is greater than the long-term average, the time is declared an event. The event is determined to end when the short-term average value decreases back to the value of the long-term average. The algorithm also looks at event parameters, such as frequency spectrum and length of event, to make sure the detected event was an earthquake and not noise (Allen,

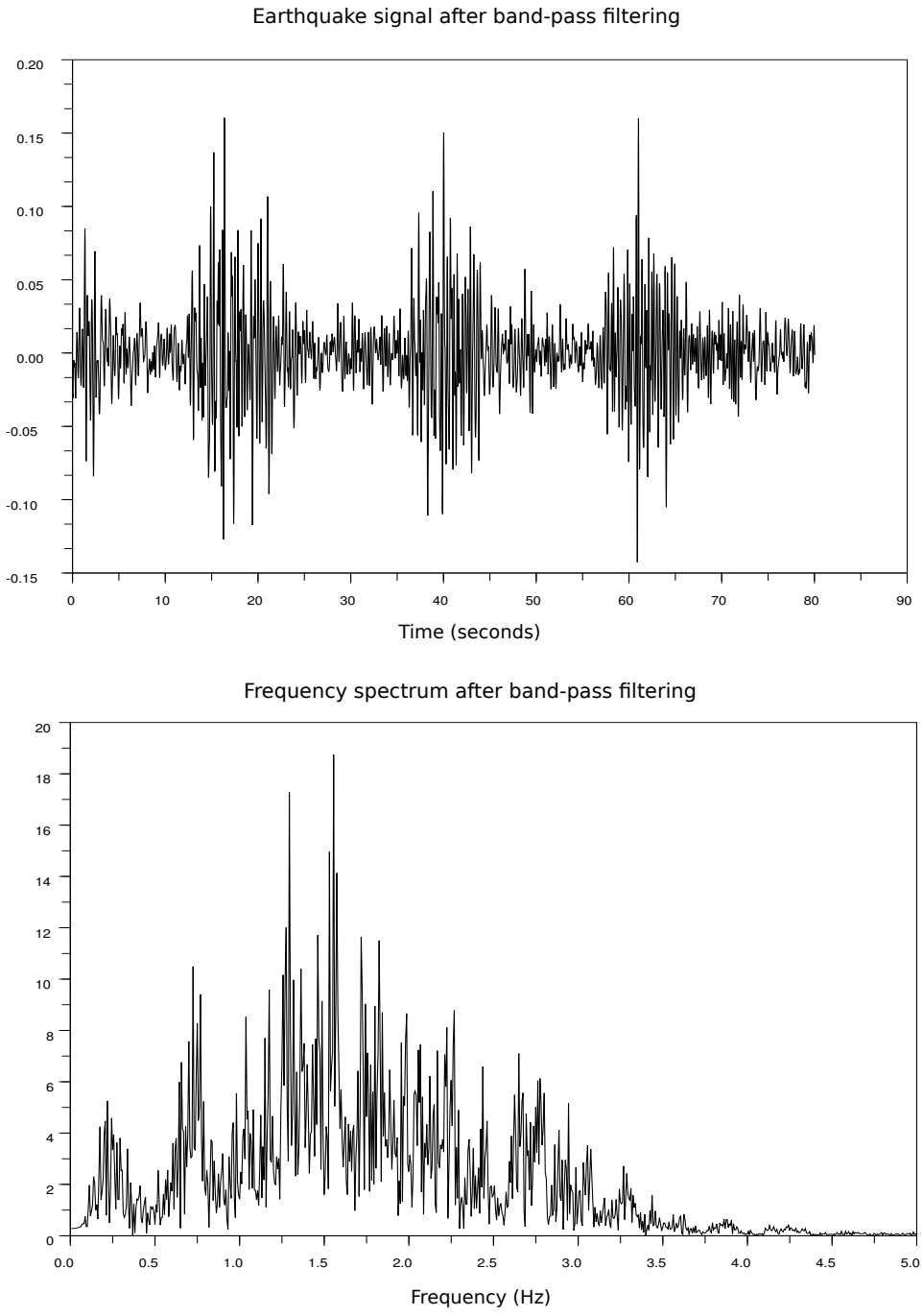

Figure 3.4: Band-pass filtering removes noise in unwanted frequency bands. This figure shows the seismic signal with reduced noise and its frequency spectrum as a result of filtering.

1978).

However, the short-term average/long-term average method was not ideal for earthquake swarms when arrival times were as short as 15 seconds apart. For this research, an algorithm was created that finds earthquakes using a forward/backward energy ratio. The code is in Appendix A.

The first step is to read in the data, set the signal mean to zero, and define the sampling interval. This algorithm uses the absolute value of the signal. To find the best ratio, I used a window size of 150 samples, or 3 seconds, since it sampling interval is 0.02 seconds. Starting with sample 151, a value for that sample is given, which is the result of the sum of the next 150 samples divided by the sum of the previous 150 samples. A predetermined threshold is chosen based on the mean and standard deviation of the energy ratios. In most cases, the threshold was the standard deviation times 4 added to the mean of the absolute value of the signal. If an energy ratio exceeds the threshold, that time is saved as a pick. Figure 3.5 shows the original signal used for the picking algorithm along with the corresponding energy ratio. The solid horizontal line in Figure 3.5 is the threshold used for picking. Once a pick is saved, the algorithm jumps ahead 12 seconds in order to prevent picking two values above the threshold for the same earthquake. The program continues searching for values above the threshold. Once all the earthquake arrival times are stored for a given file, these times are saved to a new file so that they can be used for other algorithms, such as the ones described in later sections.

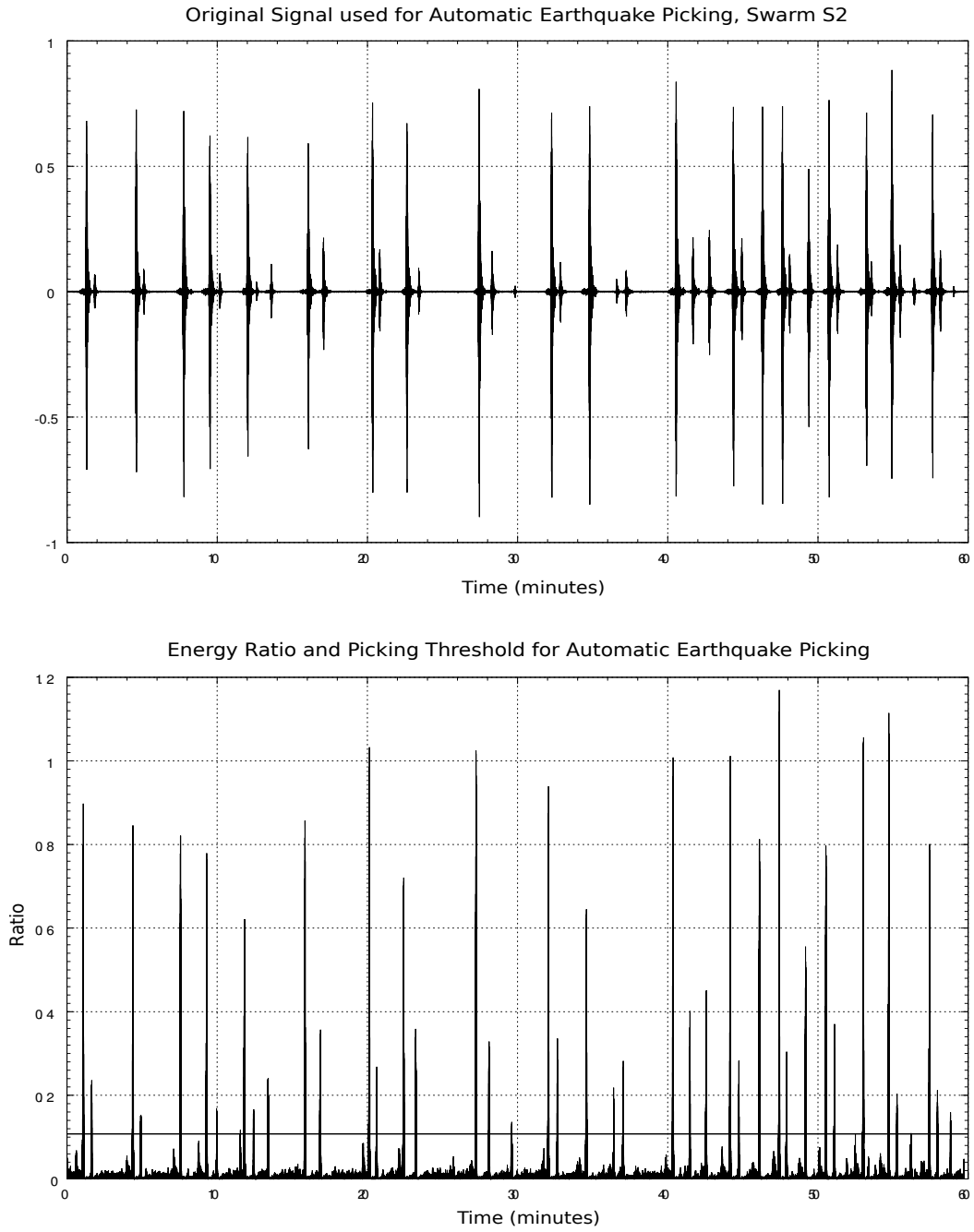

Figure 3.5: Automatic earthquake picking is done by creating a forward-backward energy ratio. If the ratio value is above a predetermined threshold (shown by the horizontal line in the bottom figure), the time is saved as the beginning of an event. This figure shows the original seismic signal, the corresponding energy ratio, and the threshold for picking.

3.3 Possible Patterns

After data were filtered and earthquake arrivals were cataloged, it was possible to search for patterns within earthquake swarms based on eruption outcome. The patterns described below include event duration and time between events in the time domain and central frequency and shape factor in the frequency domain.

3.3.1 Event Duration

The duration time of events is the strongest feature that differs between swarms that lead to eruptions and swarms that do not lead to eruptions. Duration times were calculated based on the Arias Intensity. Stafford *et al.* (2009) describe the Arias Intensity as a measure of the strength of ground motion. It is most often used in determining possible landslides or the damage that could come to structures, both as a result of earthquakes. A representation of the Arias Intensity is show in Equation 3.2, where a represents the acceleration, g is the acceleration due to gravity, and I is the resulting Intensity (Stafford *et al.*, 2009). In the case of event duration, the signal is summed over a window as a representation of the integral, as described below. The Scilab code used can be found in Appendix A.

$$I = \frac{\pi}{2g} \int a^2(t)dt \tag{3.2}$$

The first step in solving for the event duration is to read in seismic data, set the minimum time to zero, and define the sampling interval. Also, the saved earthquake arrival times are read in and the first and last pick times are defined (pmin and pmax). On average, the automatic earthquake picks were offset by ten seconds,

which is corrected at this point. The duration for each of the automatically picked earthquake arrivals is calculated. Starting with the first autopick, a 12 second time gate is created and a corresponding sampling window, which is the time divided by the sampling interval.

After the time and sampling windows are created, it is possible to calculate a value for the duration. First, the signal is squared. Then, the values within the sampling window are summed. A new variable is created where each value is the sum at that point divided by total sum and multiplied by 100. This new variable is an expression of the energy of the earthquake signal as a percentage, as shown in Figure 3.6.

Now that the Arias Intensity is solved for, it is possible to calculated the event duration. According to Kramer (1996), the duration is the time it takes for the Arias Intensity to increase from 5% to 95%. Figure 3.6 shows the arias intensity with the 5% and 95% threshold lines. After the duration is found for a single event, the time is saved and the same process continues with the next earthquake pick time until there are no times left. In some cases, the last earthquake pick time was less than 12 seconds from the end of the file, so the value was ignored.

3.3.2 Time Between Events

The time between events was calculated from the automatic earthquake picking saved times. The first step is to read into Scilab the earthquake pick times. Then, it's as simple as creating a new variable that is the difference between pick times for all of the recorded earthquakes. Lastly, the new variable is saved as a new file.

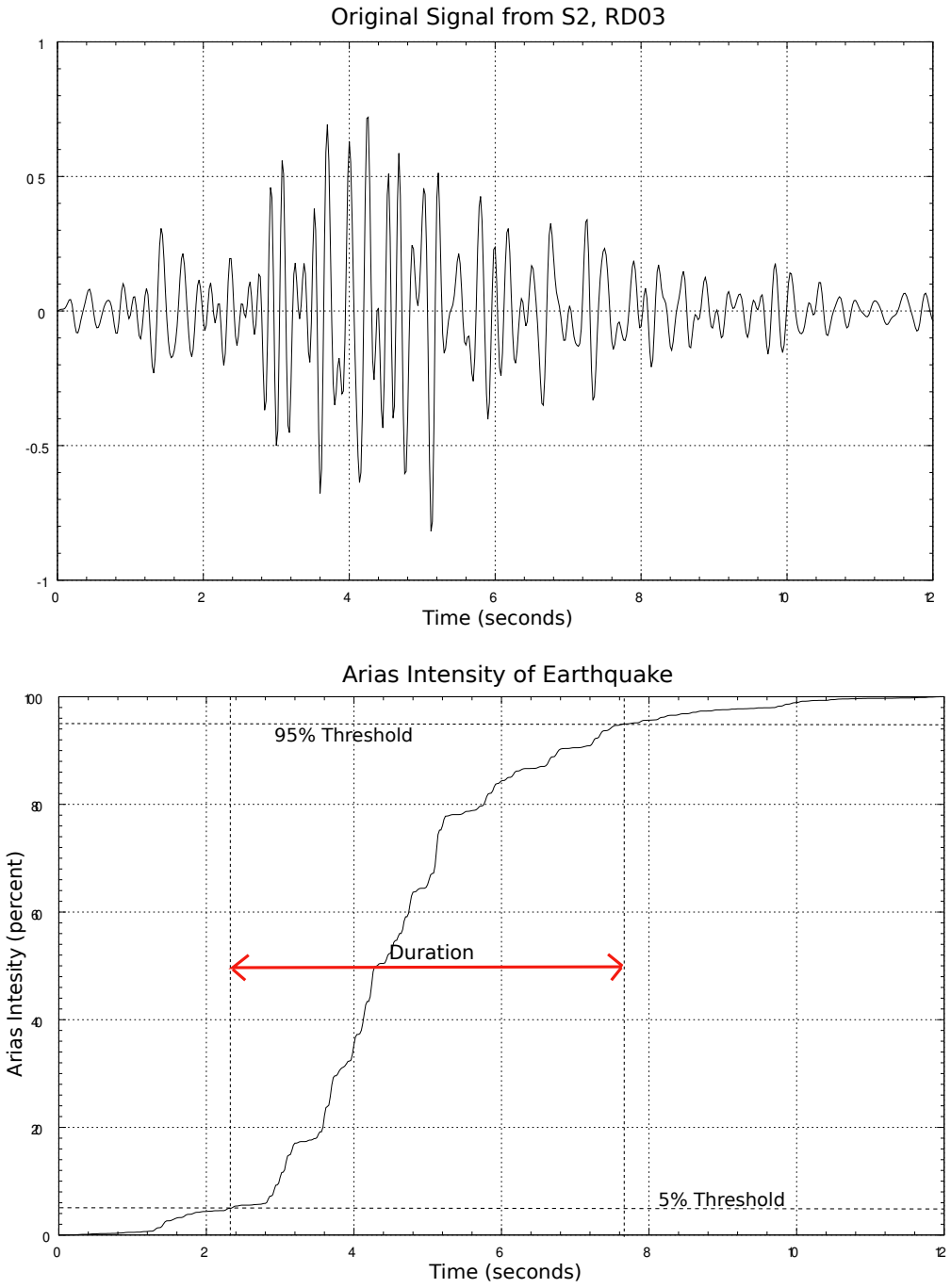

Figure 3.6: The duration of an earthquake was computed based on the arias intensity for the signal shown. The time it takes for the intensity to change from 5% to 95% is the resulting event duration.

3.3.3 Power Spectrum from Auto-Correlation

The power spectrum from the auto-correlation of a signal was computed in order to look for patterns in the frequency spectrum. The features compared in the frequency spectrum include the central frequency and shape factor of a high-order correlation.

The goal of the auto-correlation is to compare a signal to itself with a defined lag in order to find similarities within a signal. Because swarm events have similar waveforms, they should stand out in this process.

The first step in computing the auto-correlation is to read in the signal. For each computation, one hour of data was used to get an average value for each hour. The mean of the signal and the time minimum should both be set to zero if they haven't been already and the sampling interval is computed. The length of the lag for the auto-correlation is also defined at this point. For the high-order correlations, a lag of 1000 samples was used. The auto-correlation of the signal is computed and the levinson equation is solved for the order of process using the corr and lev commands in Scilab, respectively.

The intended result of the autocorrelation of a signal is the power spectral density function. Bendat and Piersol (1971) explain that this function is the fourier transform of the autocorrelation, and it describes the overall frequency composition of the data. Therefore, if seismic data consists of a repetitive signal, the power spectral density function should be a representation of the frequency spectrum of the repetitive signal.

After a power spectral density function was computed for each hour of data, the search for patterns could also continue in the frequency spectrum.

3.3.4 Central Frequency

As previously described, the power spectral density function was computed for each hour of earthquake swarm data. Then, the central frequency was calculated for each spectrum. The central frequency is a representation of the frequency where the power spectral density is most concentrated (Kramer, 1996).

The first step in computing the central frequency is to define ω_0, ω_1, and ω_2, where ω_n represents the frequency spectrum to the *nth* power. Central frequency is represented by Equation 3.3 and Ω is defined by Equation 3.4, where *G(λ)* is the amplitude at each frequency.

$$\Omega = \sqrt{\frac{\lambda_2}{\lambda_0}} \tag{3.3}$$

$$\lambda_n = \int \omega^n G(\omega) d\omega \tag{3.4}$$

3.3.5 Shape Factor

The shape factor also works with the power spectral density functions. It is a representation of the dispersion of the spectrum about the central frequency (Kramer, 1996). Values for the shape factor range from 0 to 1 with higher values corresponding to a larger dispersion. Shape factor (δ) is defined by Equation 3.5.

$$\delta = \sqrt{1 - \frac{\lambda_1^2}{\lambda_0 \lambda_2}} \tag{3.5}$$

CHAPTER 4:

RESULTS

This chapter explains the patterns, or lack of, in earthquakes swarms. The patterns explored and discussed below include event duration, time between events, central frequency, and shape factor.

4.1 Event Duration

The event duration was the feature with the biggest difference between swarms that preceded eruptions and swarms that did not. Swarms that preceded eruptions had shorter event duration times, on average, than swarms that did not precede eruptions. Also, statistical analysis shows swarms that did not precede eruptions had less variance in duration times. Table 4.1 shows duration values for all of the swarms. Ketner and Power (in press) found similar results for event duration times with mean times falling between 5-10 seconds.

Figures 4.1 - 4.7 show results from the swarms and include both individual duration times for each event along with the mean duration times per hour with the exception of S3. Since S3 only lasted about an hour, the mean and median times are not shown on Figure 4.3.

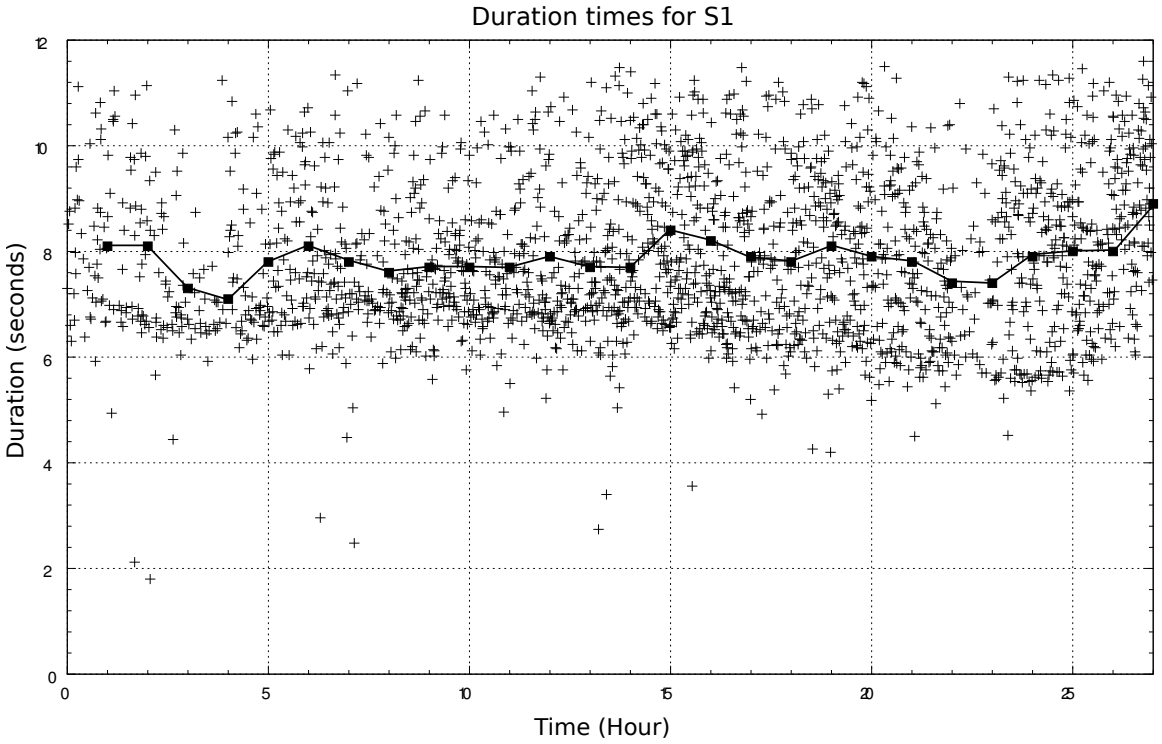

Figure 4.1: The 3/22-3/23/2009 earthquake swarm lasted 27 hours and preceded the first explosion of the eruption. This figure shows the individual duration times for events that occurred during the swarm. Mean duration times per hour are shown as connected square points.

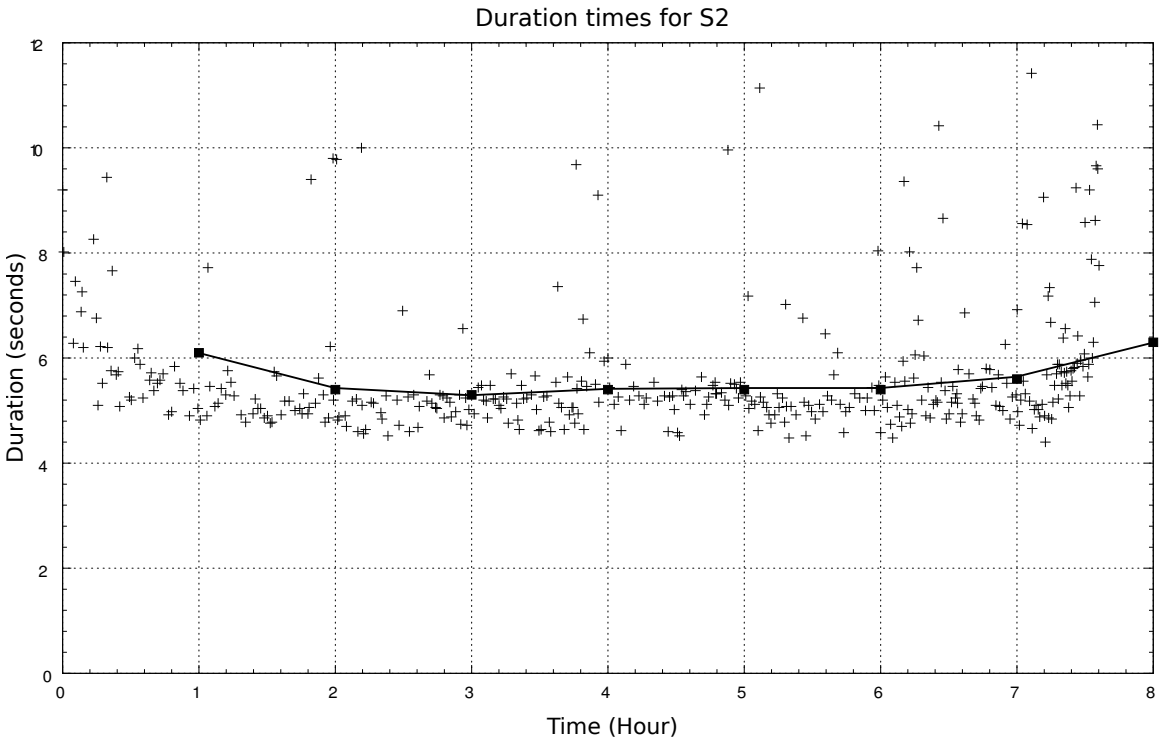

Figure 4.2: Duration times for earthquakes that occurred during S2 (preceded explosion) were on average, the shortest. They do increase toward the end of the swarm just before erupting. Mean duration times per hour are shown as connected square points.

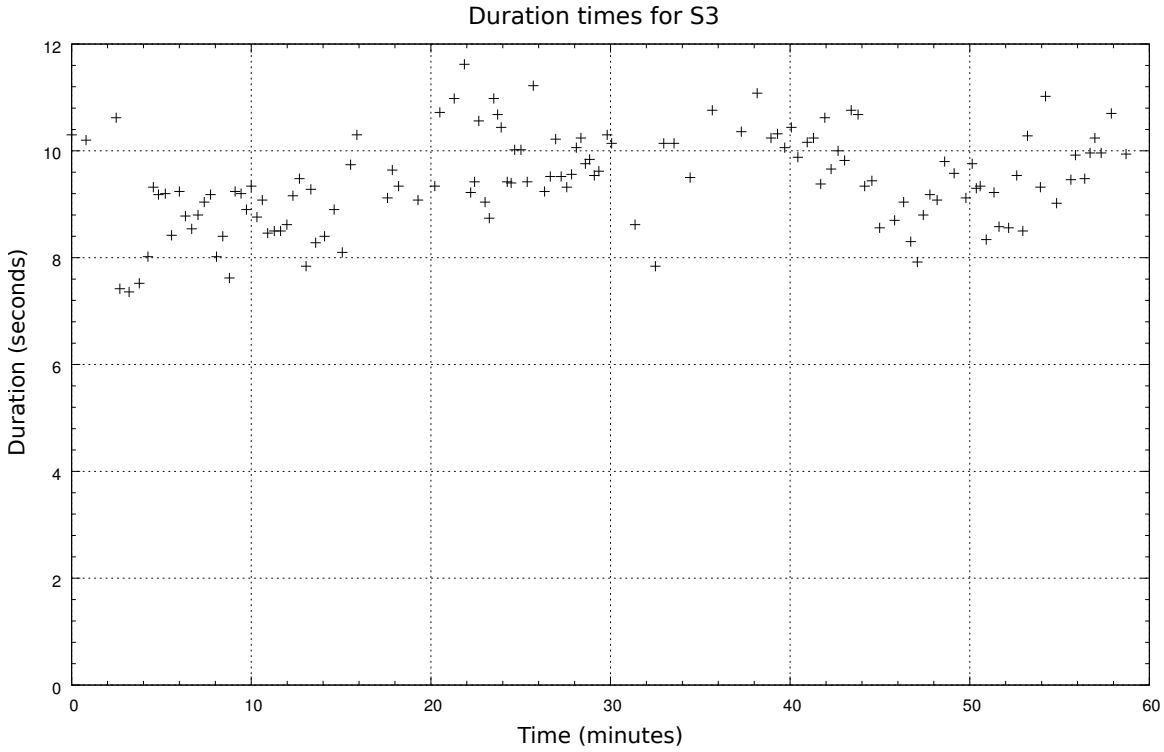

Figure 4.3: Because S3 (no explosion) lasted only about an hour, calculated duration times are shown for each event only. The mean duration value for the swarm was 9.40 seconds.

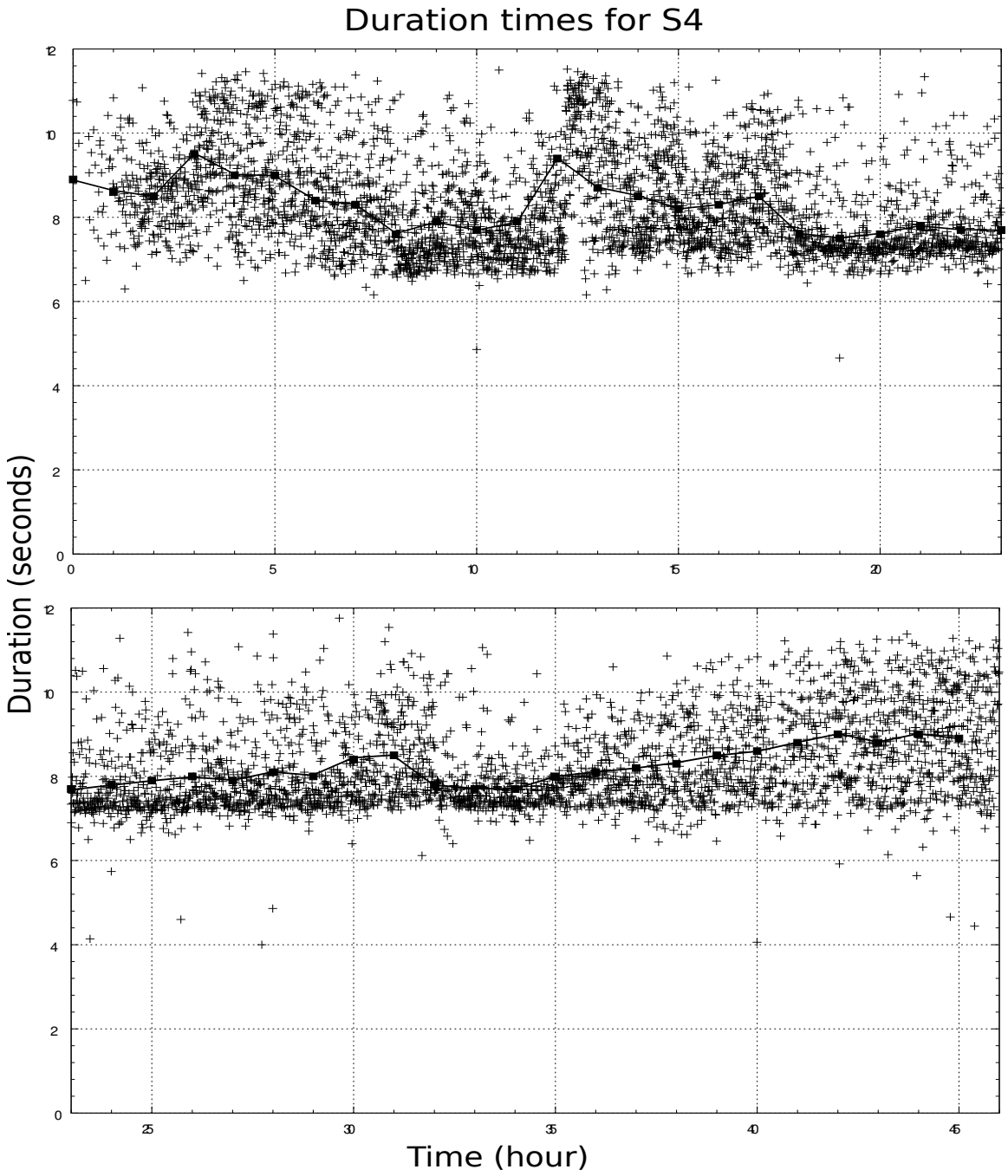

Figure 4.4: Duration event times and hourly mean values for S4. Individual duration times are shown as a (+) and mean times are shown as connected solid squares. This swarm preceded an explosive eruption.

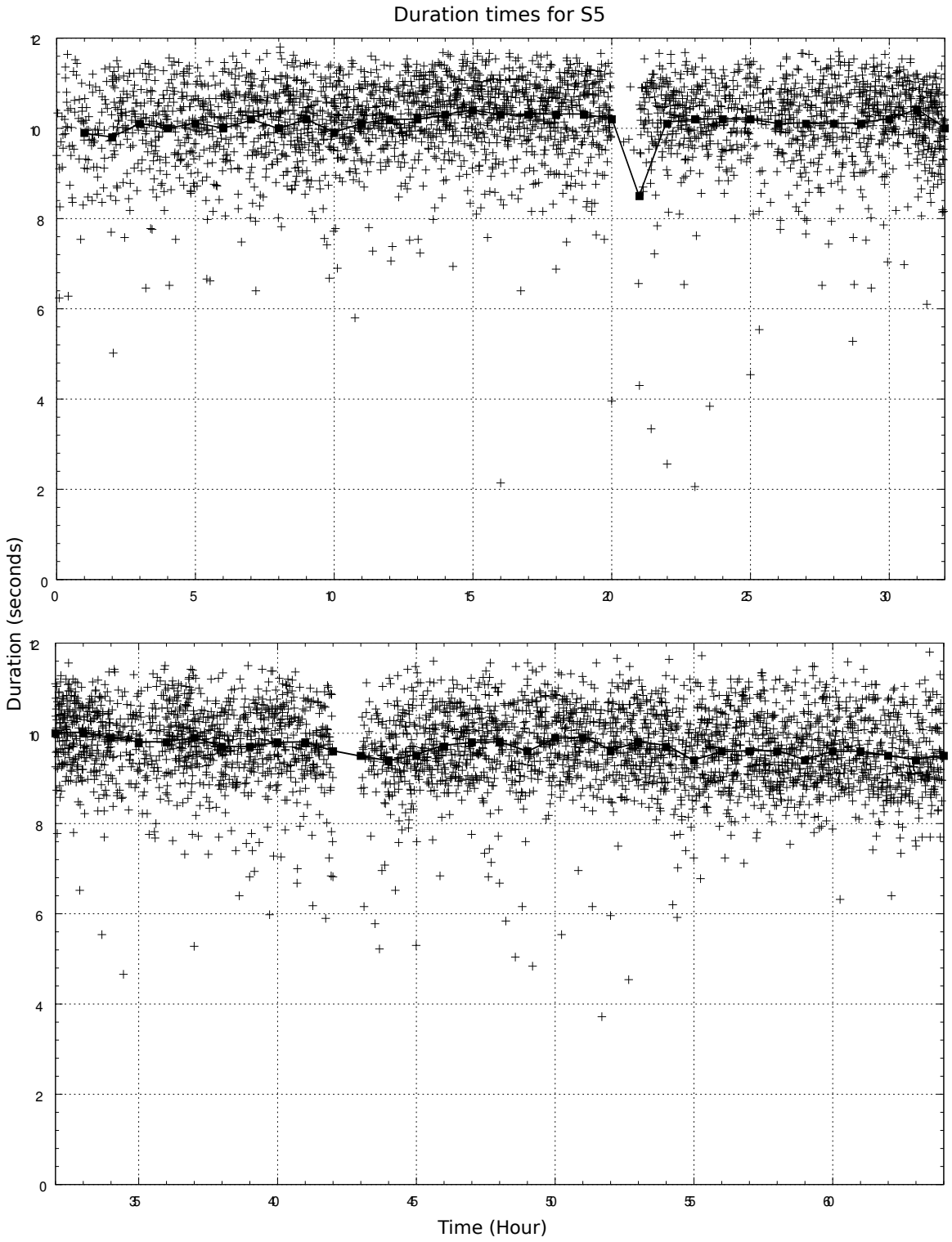

Figure 4.5: Individual and hourly mean duration times for the first 64 hours of S5. S5 had the longest duration times, on average, and it did not precede an explosive eruption.

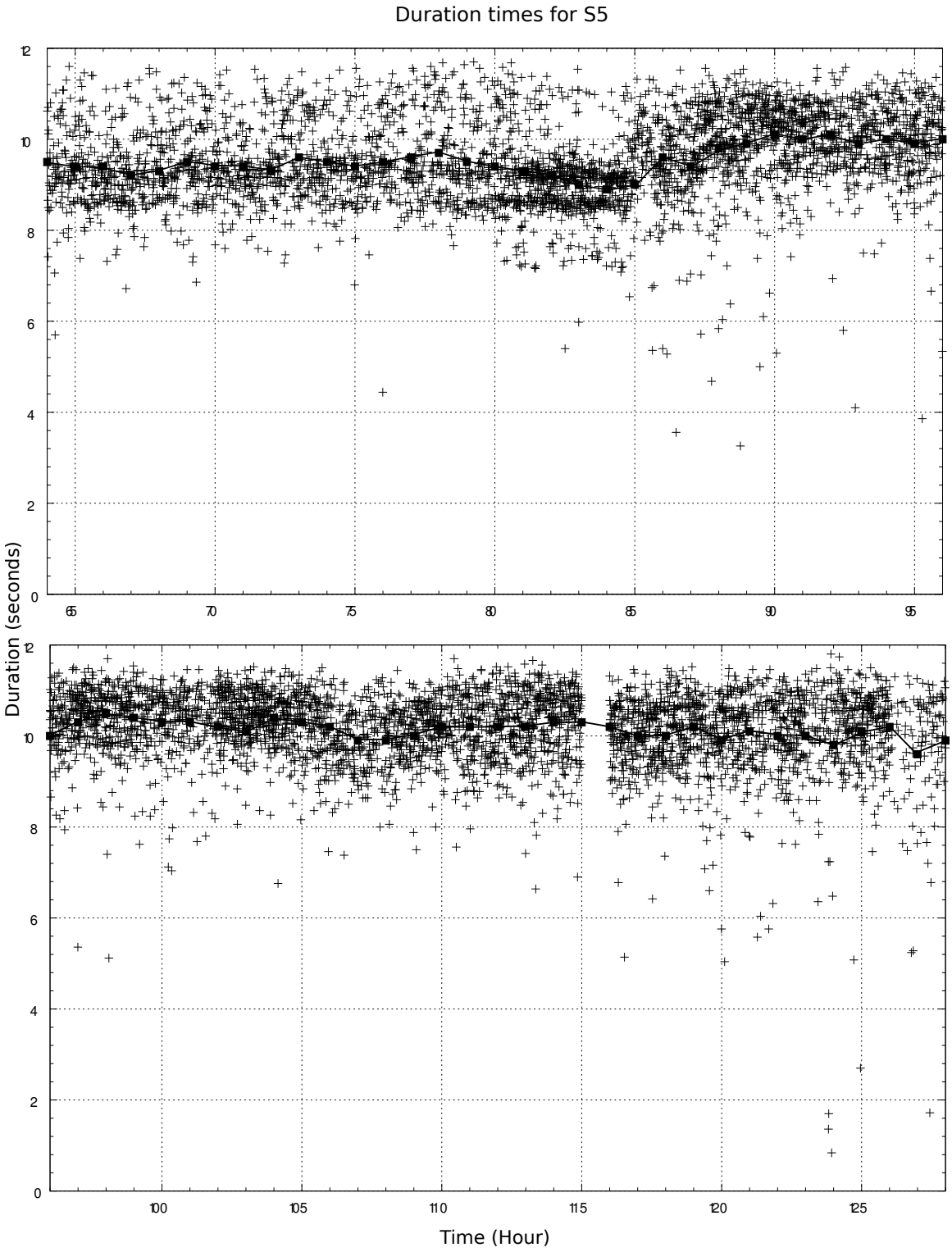

Figure 4.6: Individual and hourly mean duration times for the second 64 hours of the LP earthquake swarm occurring from 5/2/2009-5/10/2009.

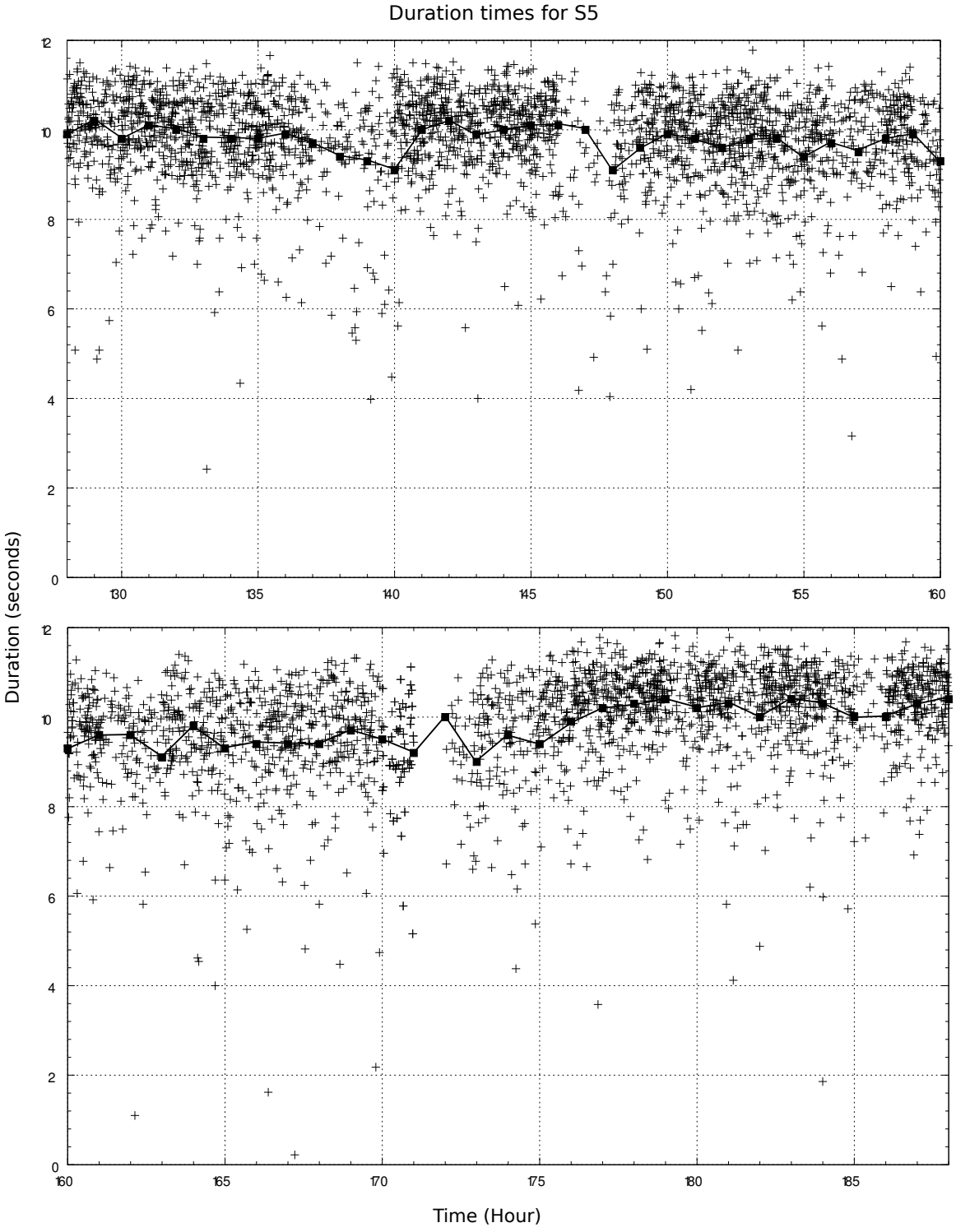

Figure 4.7: Individual and hourly mean duration times for the last 60 hours of the LP earthquake swarm occurring from 5/2/2009-5/10/2009.

Swarm	S1	S2	S3	S4	S5
Outcome	Eruption	Eruption	No Eruption	Eruption	No Eruption
Duration Mean	7.85	5.61	9.40	8.28	9.87
Duration Median	7.60	5.32	9.41	8.09	10.0
Duration St. Dev	1.41	1.11	0.86	0.97	0.98

Table 4.1: Duration times were calculated for each swarm event. Shown here are the average times for the entire swarms along with results of a statistical analysis of duration times. Average duration times and statistical values show a pattern between swarms that precede eruptions and swarms that do not.

4.2 Time Between Events

As discussed in Chapter 3, the amount of time between events was explored as a possible feature. Unlike duration times, there is not a pattern between how often events occur and whether or not the swarm will lead to an eruption, at least for the 2009 Redoubt eruption. Values were high for S1 and S2 and low for S3-S5. These results are slightly different from the values reported in Ketner and Power (in press), which all have mean values around 30 seconds. This could be due to different approaches to picking earthquake arrivals. Ketner and Power (in press) found event rate (inverse of time between events) was the most successful characteristic in predicting explosive eruptions. Table 4.2 and Figures 4.8 - 4.14 show the results from this study for each swarm. The figures include individual times between events along with hourly mean values, shown by connected black squares.

4.3 Central Frequency

Central frequencies of the power spectrum from high-order autocorrelations were calculated hourly. Average values from each swarm, shown in Table 4.3, show a slight

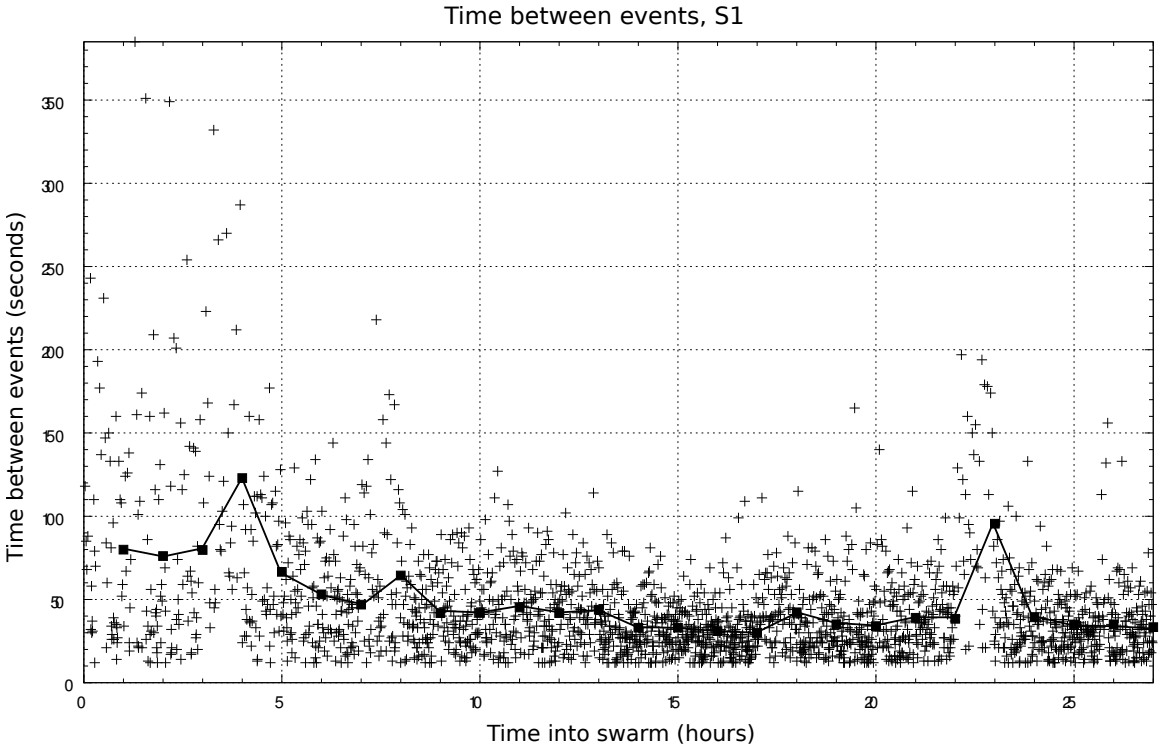

Figure 4.8: Because the number of events increases closer to the time of eruption, the time between events decreases over time. Each individual value is shown, and hourly average values are shown in connected squares.

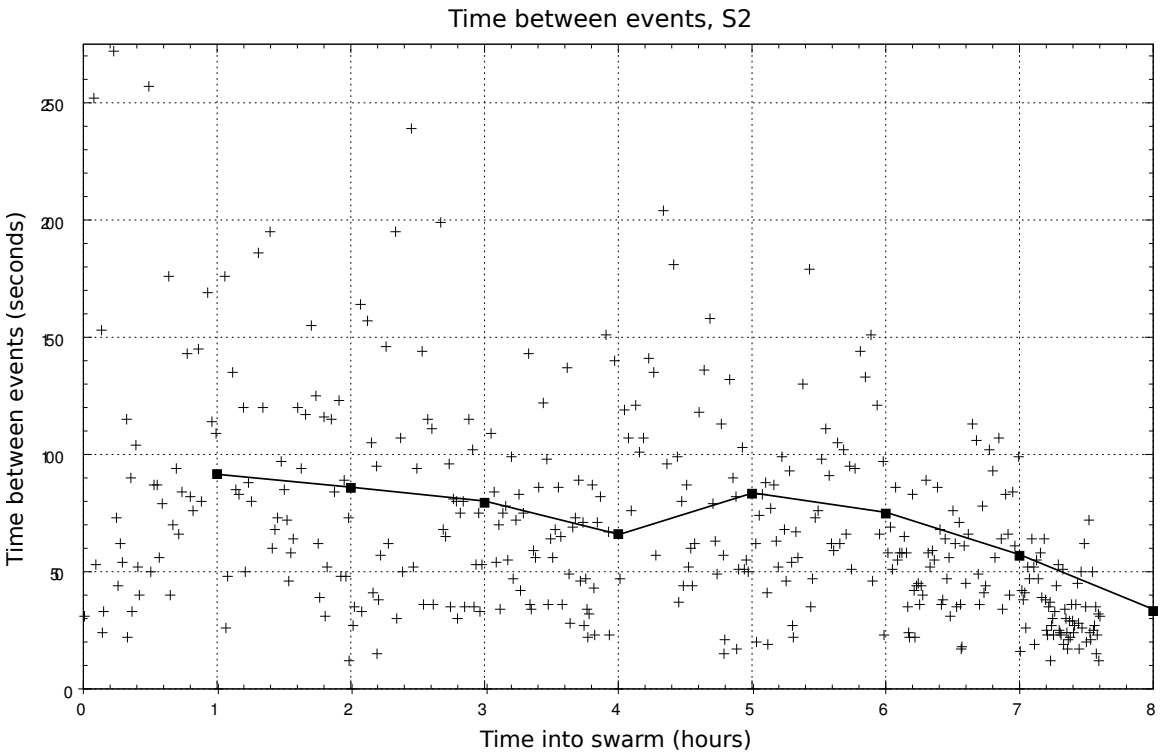

Figure 4.9: Time between events for S2 decreases over time since the number of events increases closer to the eruption. A significant decrease in interval times occurred in the hour before eruption as the number of events increases.

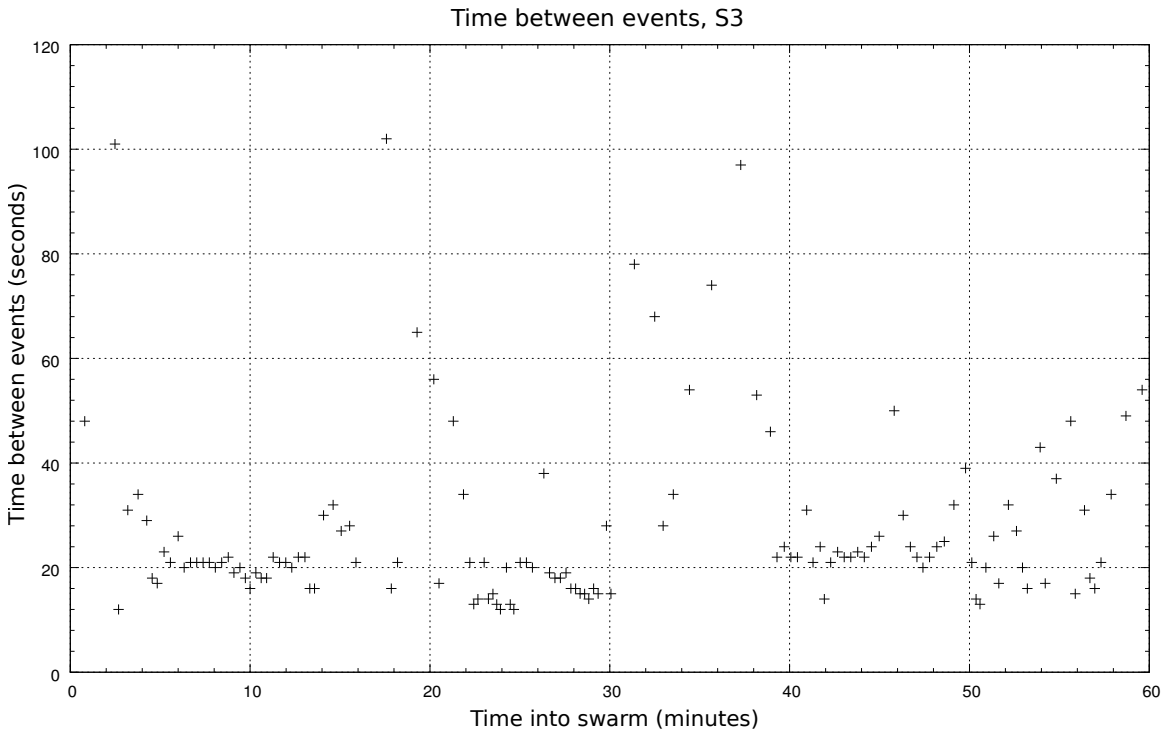

Figure 4.10: Most of the inter-event times for S3 are around 20 seconds. Values increase towards the end as the swarm dies off since there was no eruption.

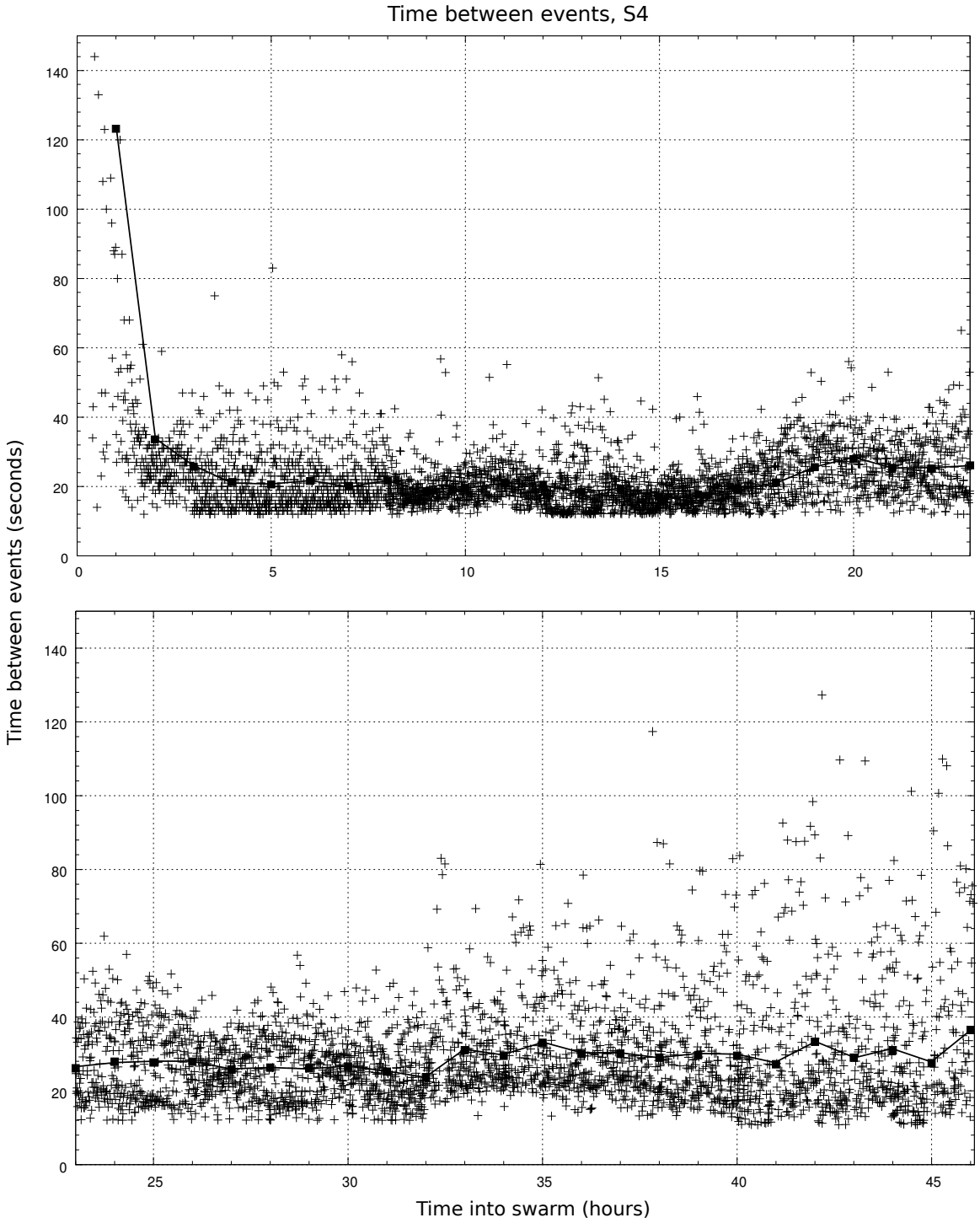

Figure 4.11: Unlike the other two swarms that preceded an eruption, interval times from S4 increased towards the end of the swarm. These values were the second shortest values, on average. These results are anomalous compared to S1 and S2.

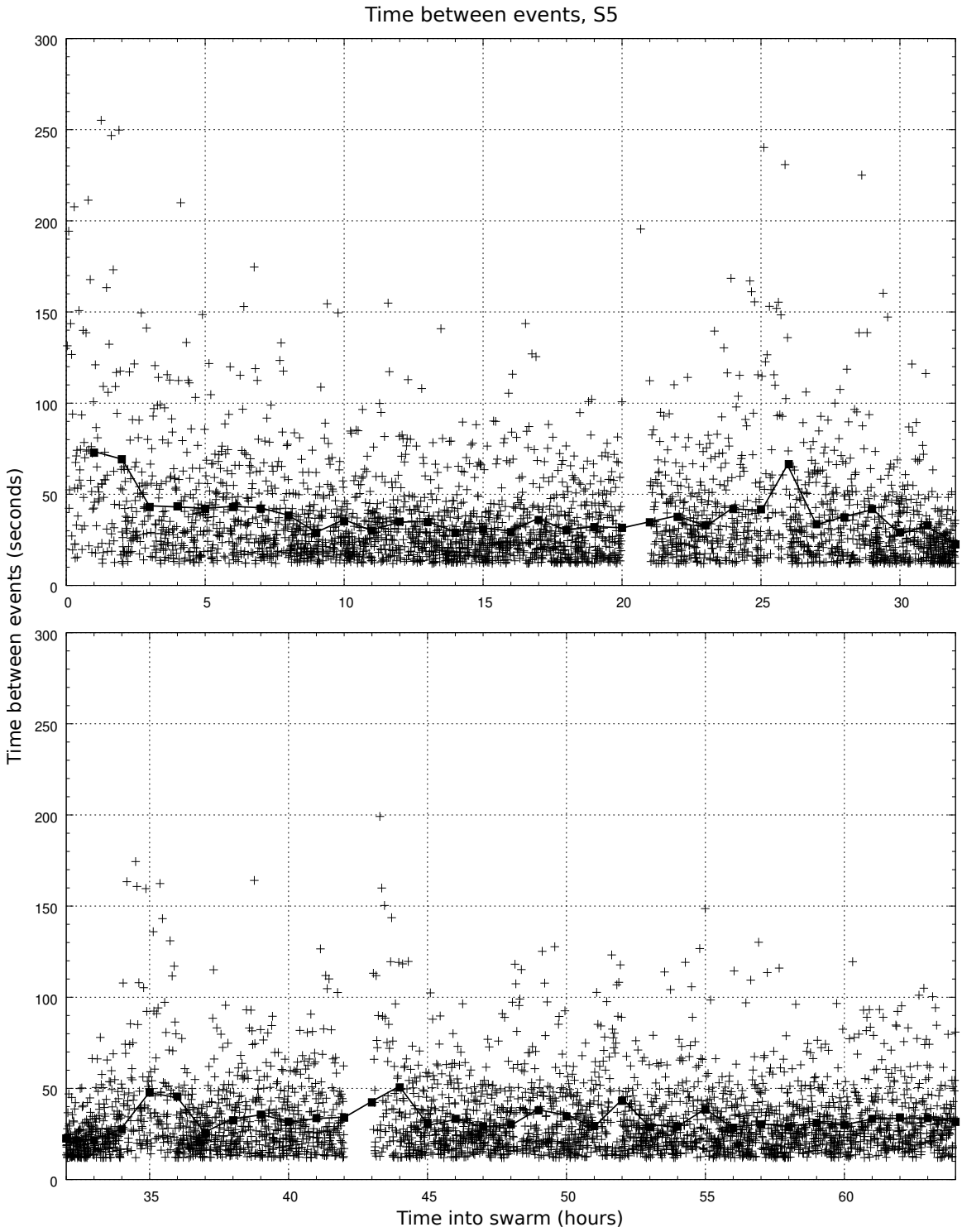

Figure 4.12: For the first 64 hours of the swarm, the majority of interval times fall between 20 and 100 seconds. Values are highest at the beginning of the swarm since the onset was gradual.

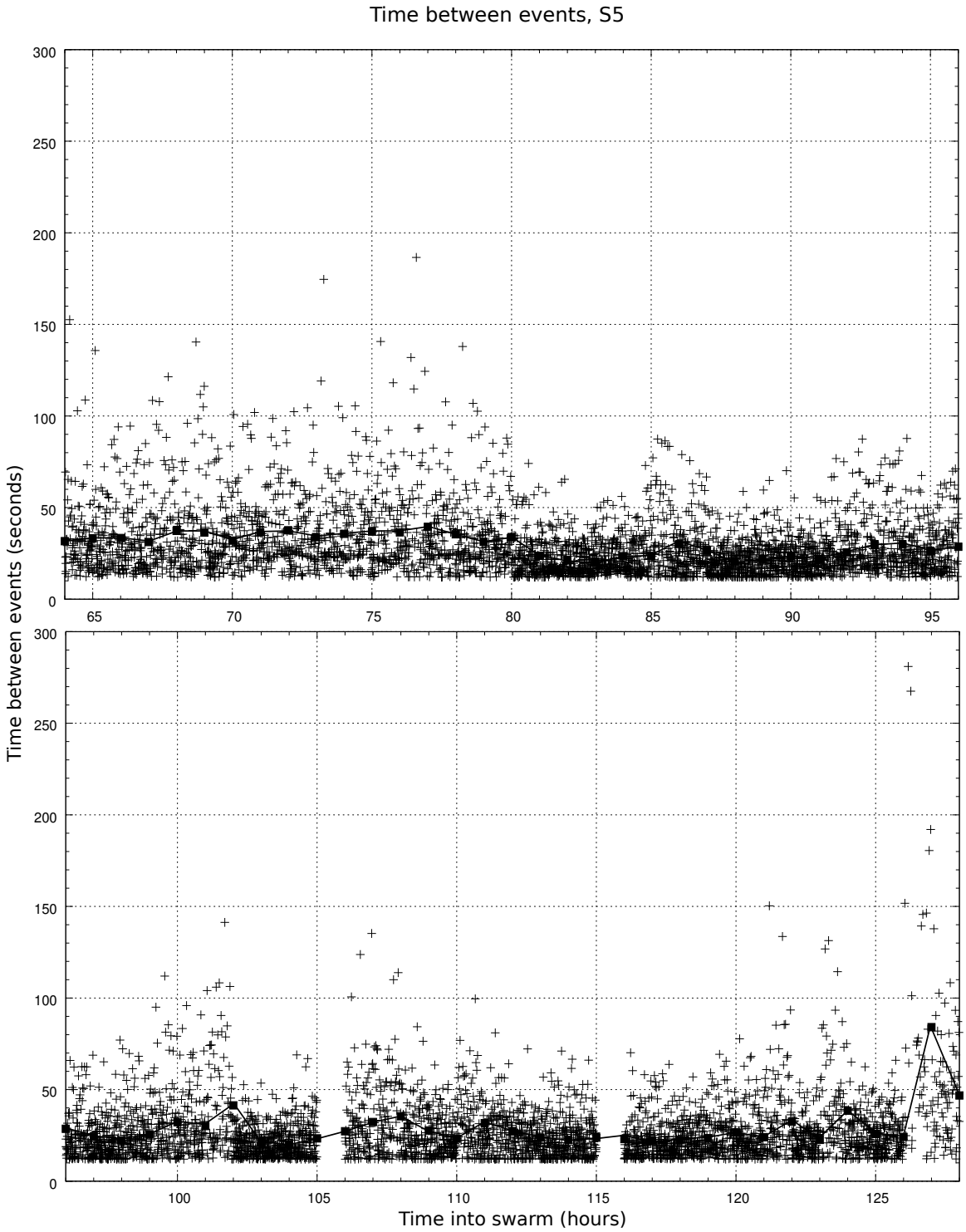

Figure 4.13: Values for S5 were shortest in the middle of the swarm. A distinct decrease in times occur at hour 80, which follows a rockfall event.

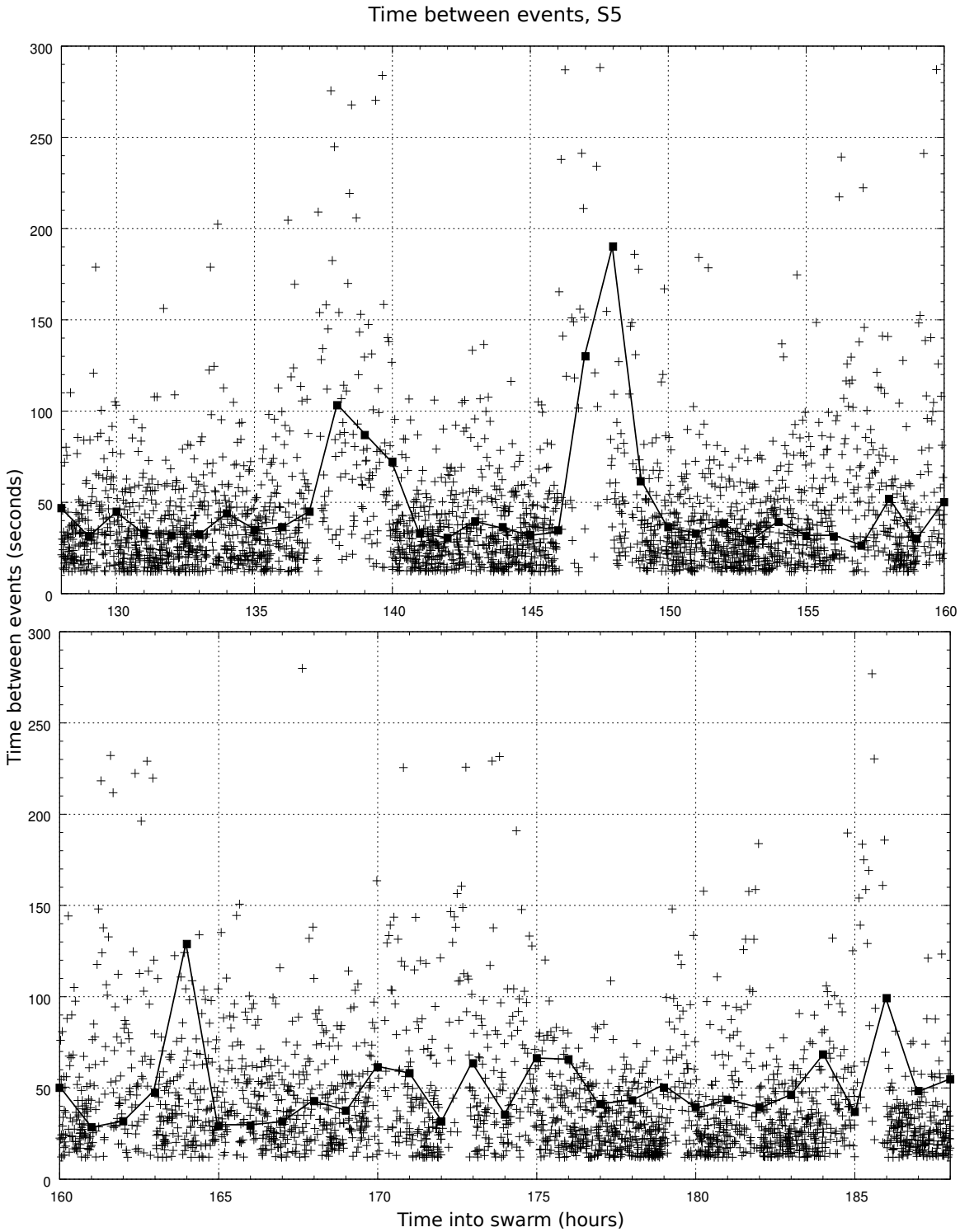

Figure 4.14: The end of S5 had the highest interval values. Since there was no eruption, the swarm died off and the time between events were higher. Spikes in values can be explained by noisy data, resulting in poorly picked events.

Swarm	S1	S2	S3	S4	S5
Outcome	Eruption	Eruption	No Eruption	Eruption	No Eruption
Time Between Mean	50.31	71.36	26.90	27.70	38.17
Time Between Median	41.76	66.00	21.00	24.35	30.90
Time Between St. Dev	32.35	39.57	17.03	12.87	26.32

Table 4.2: The interval time between events were calculated for each swarm. The mean, median, and standard deviation values are shown here. With the exception of S4, swarms that do not lead to an eruption tend to have lower values.

trend between swarms that precede eruptions and those that do not. Specifically, two of the swarms that preceded an eruption (S1 and S2) had higher mean values. However, S4, which also preceded an explosion had the same mean value as S2, which did not. S5 (no explosion) had the lowest mean value out of all swarms. The following table and figures show the statistical analysis and hourly results for each swarm, respectively.

Central frequency values can be compared to peak frequency values from Ketner and Power (in press). Even though different methods were used to compute frequency values, results should be relatively comparable. Ketner and Power (in press) found peak frequency values around 5 Hz for S1, S3, and S5. Frequency values were lower for S2 and higher for S5. These results are different from the results shown in Table 4.3. Central frequency values are the highest for S2 with the other swarms between 4.27 and 3.94 Hz. However, there are some trends within each swarm that are comparable to results from Ketner and Power (in press). For example, both studies find a general decrease in frequency values with time for S4, shown in 4.18. Also, both studies show a switch from decreasing to increasing frequency trends around hour 90 for S5, which is when a rockfall event occurred.

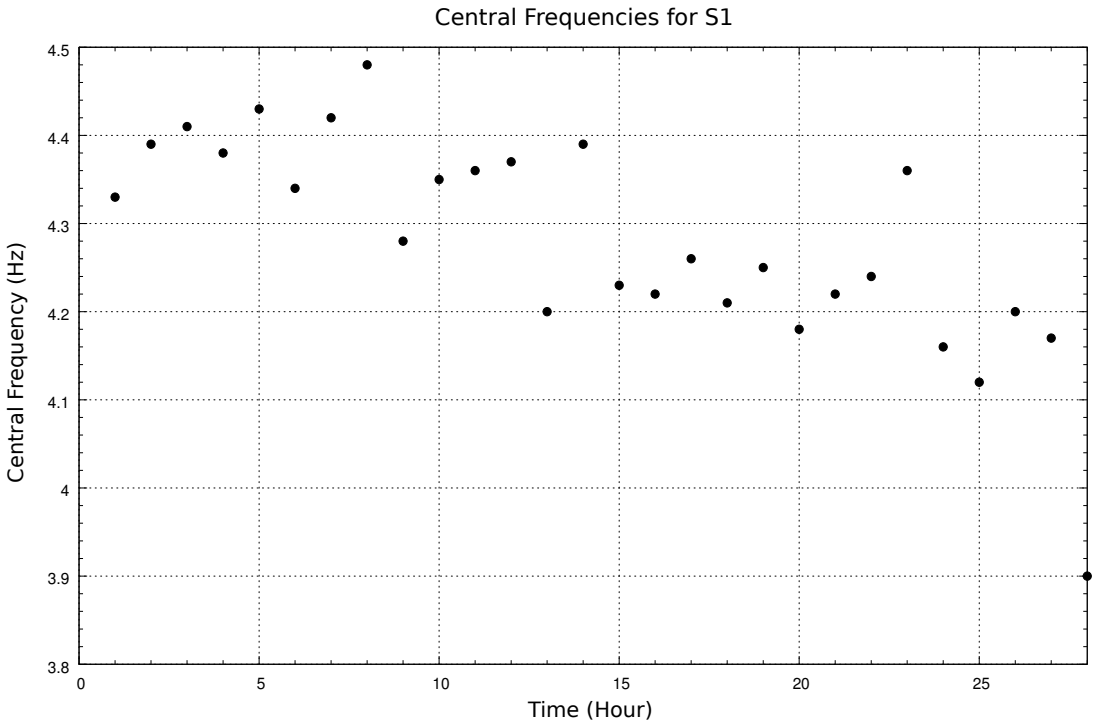

Figure 4.15: Central frequency values for S1 (eruption) are relatively high with a lower variance than most of the other swarms. There is a slight decrease in central frequency values over time with the lowest value occurring in the hour before the eruption.

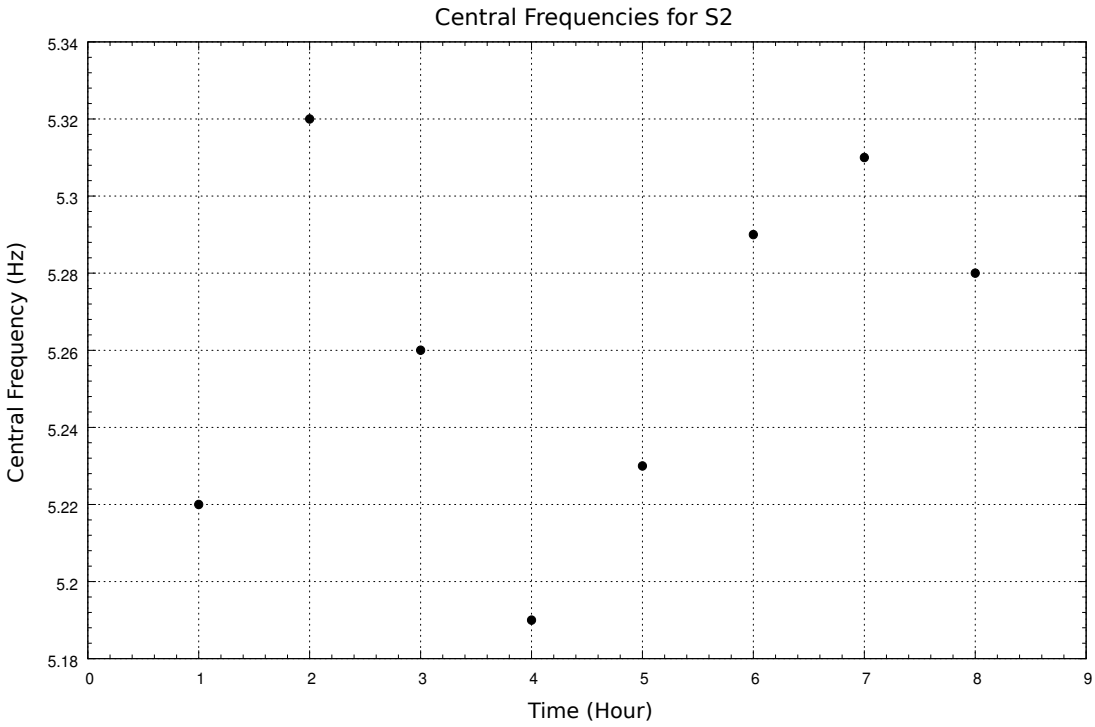

Figure 4.16: Central frequency values are the highest for S2 (eruption) out of all the swarms and has the lowest standard deviation. S2 values lack an increasing or decreasing trend over time.

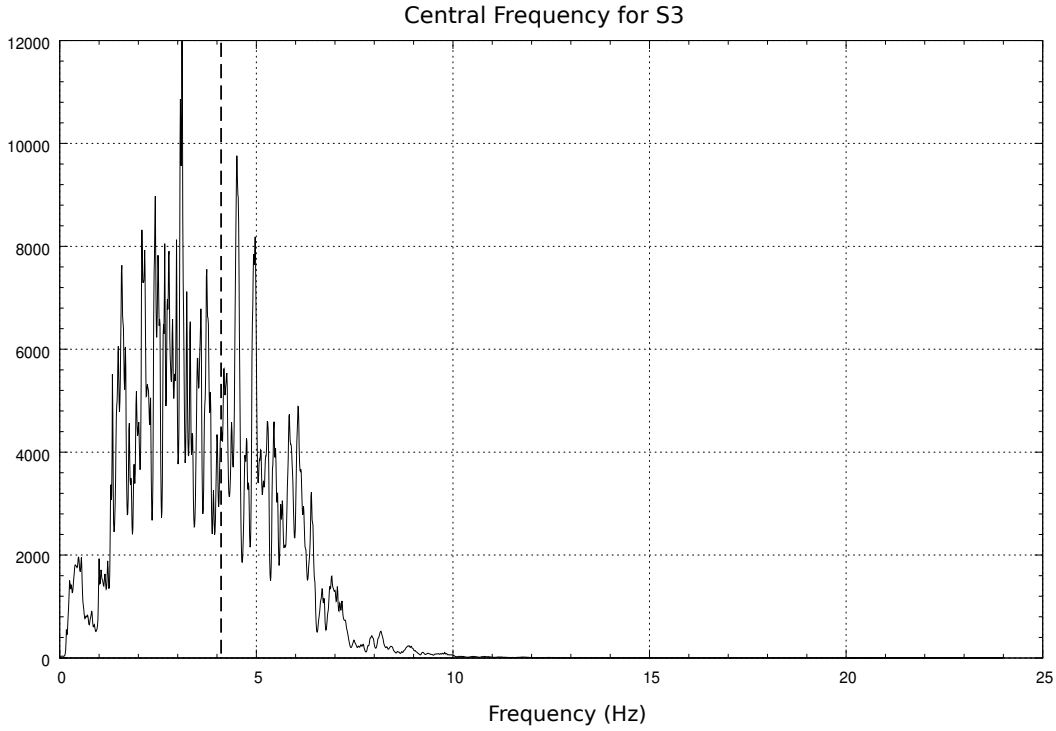

Figure 4.17: Because S3 (no eruption) contains only one hourly central frequency value, the power spectrum from the high-order autocorrelation is shown. The central frequency is 4.14 Hz and is shown by a bold dashed vertical line. Since there is only one value for S3, the standard deviation is not applicable.

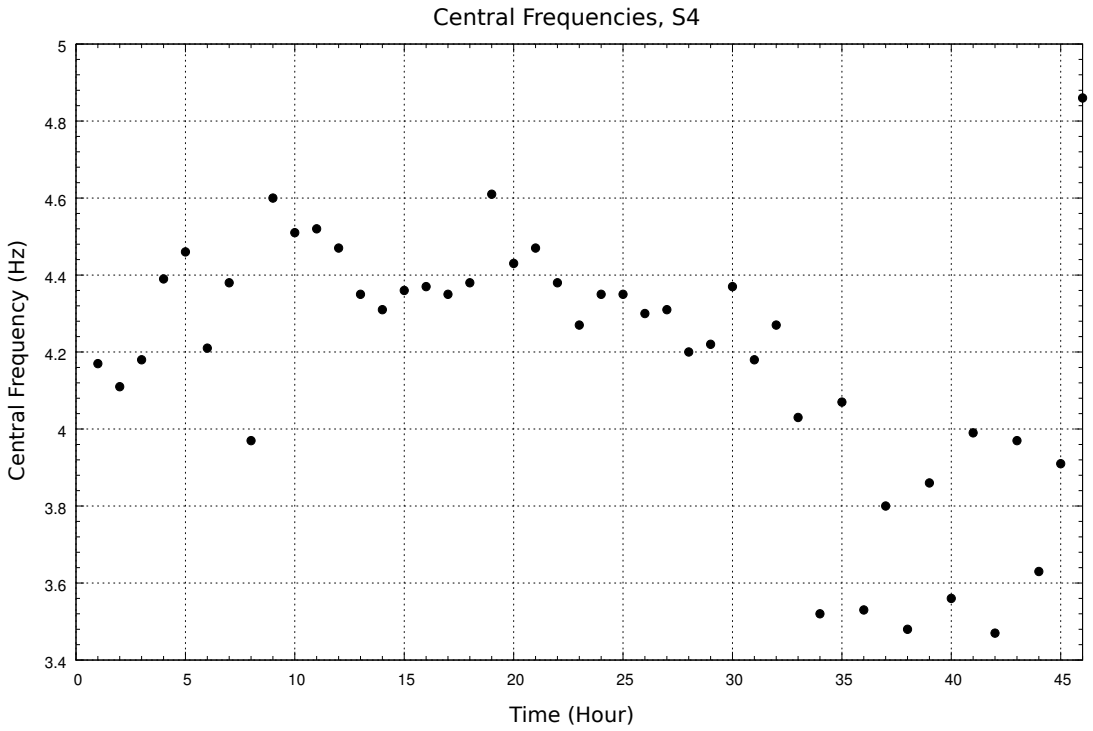

Figure 4.18: Central frequency values for S4 (eruption) were about an average for the whole eruption. However, there was the highest standard deviation in values from S4. There is a general decrease in values over time, with the exception of the hour before eruption when the highest value occurs.

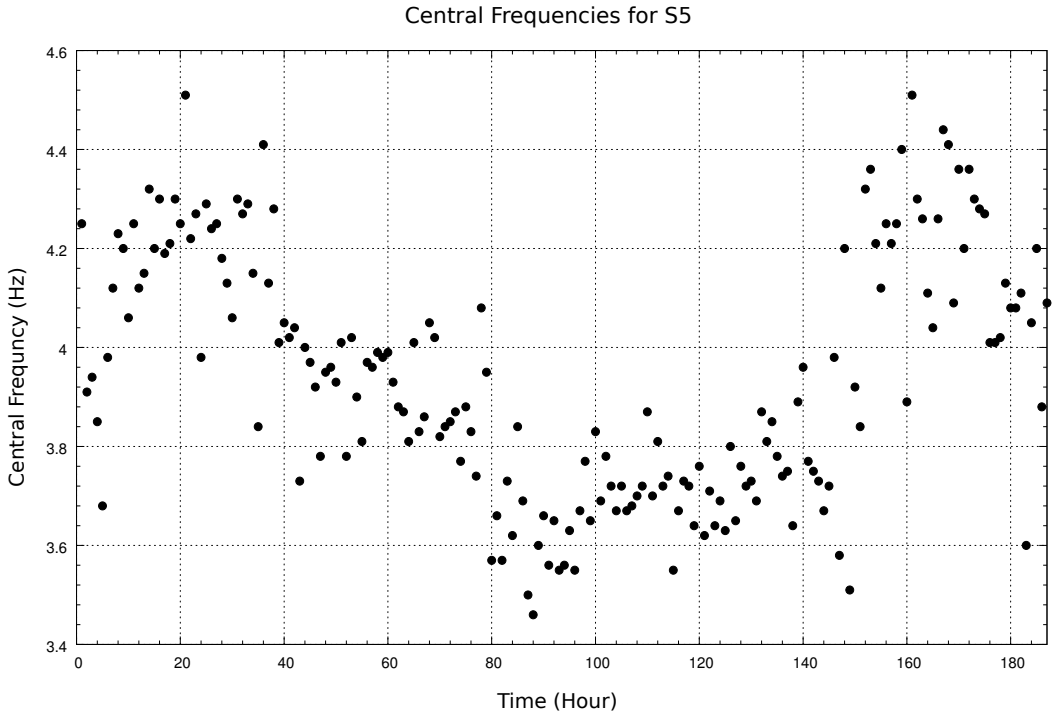

Figure 4.19: S5 (no eruption) had the lowest central frequency values of all the swarms with a mean of 3.94 Hz and a fairly large standard deviation. There is a sinusoidal trend to the values, which peak around 20 and 160 hours into the swarm.

Swarm	S1	S2	S3	S4	S5
Outcome	Eruption	Eruption	No Eruption	Eruption	No Eruption
CF Mean	4.27	5.26	4.13	4.13	3.94
CF St. Dev	0.15	0.04	n/a	0.40	0.24

Table 4.3: Central frequency values were higher for two of the three swarms that preceded explosions, as shown here. Because there is only one central frequency value for S3, the standard deviation is not applicable.

4.4 Shape Factor

As discussed in Chapter 3, the shape factor was calculated from high-order autocorrelation power spectrums. Shape factor values range from 0 to 1 and represent the spread of the frequency spectrum. Shape factor values did not change much for the different swarms, as shown in Table 4.4. Three of the swarms, one of which preceded an eruption, all had the same mean value of 0.44. Figures 4.20 - 4.23 show hourly shape factor values for all the swarms with the exception of S3, which only had one hourly value of 0.44.

Swarm	S1	S2	S3	S4	S5
Outcome	Eruption	Eruption	No Eruption	Eruption	No Eruption
SF Mean	0.38	0.37	0.44	0.44	0.44
SF St. Dev	0.01	0.03	n/a	0.04	0.03

Table 4.4: Shape factor values tend to be lower for swarms that preceded eruptions. The exception is S4, which preceded an eruption but has the same value as S3 and S5, which did not. Because there is only one shape factor value for S3, the standard deviation is not applicable.

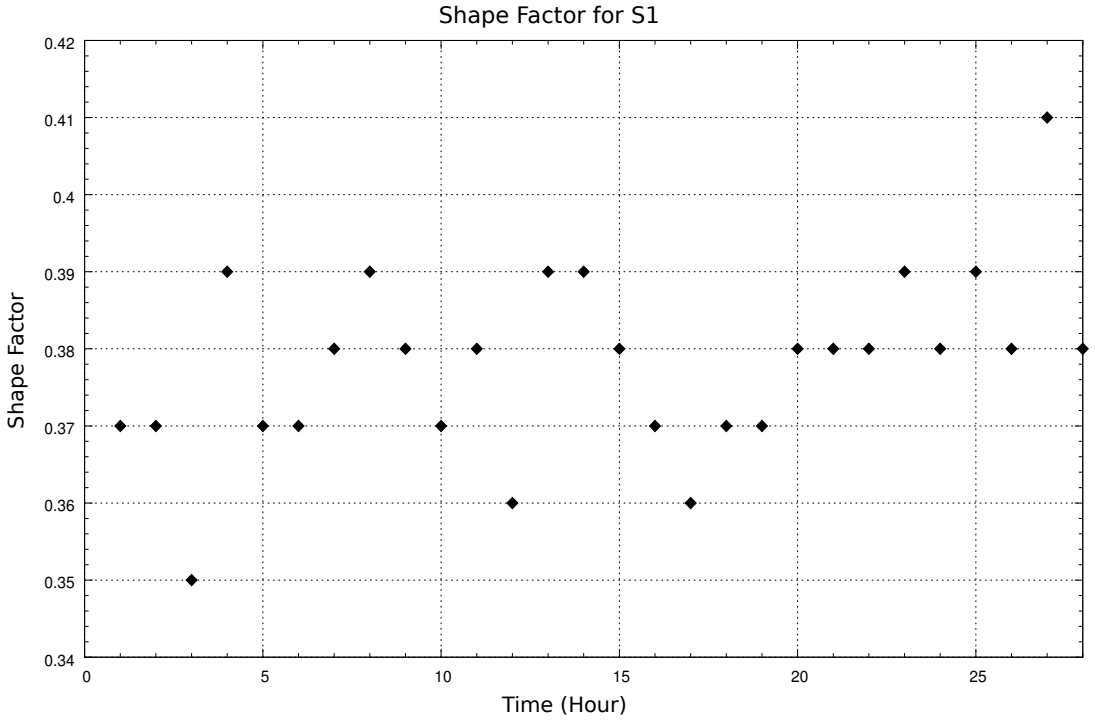

Figure 4.20: Most of the shape factor values for S1 (eruption) fall between 0.37 and 0.39 with swarm mean of 0.38 and standard deviation of 0.01.

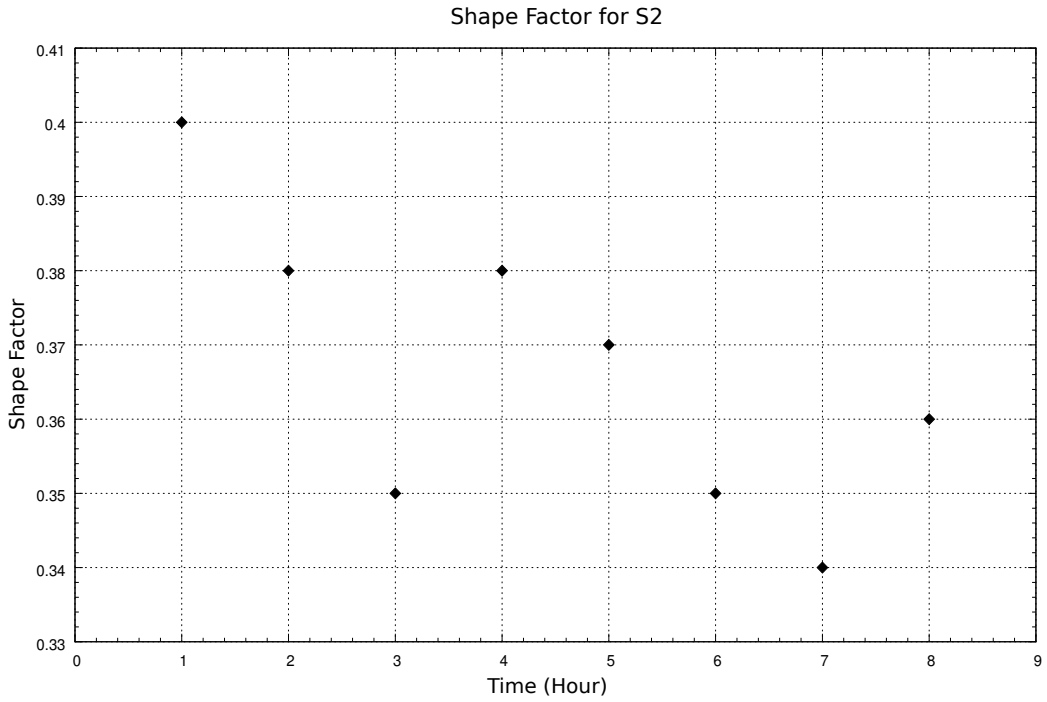

Figure 4.21: Shape factor values for S2 (eruption) fall between 0.40 and 0.34 and tend to decrease with time into the swarm. The shape factor mean and standard deviation were 0.37 and 0.02, respectively.

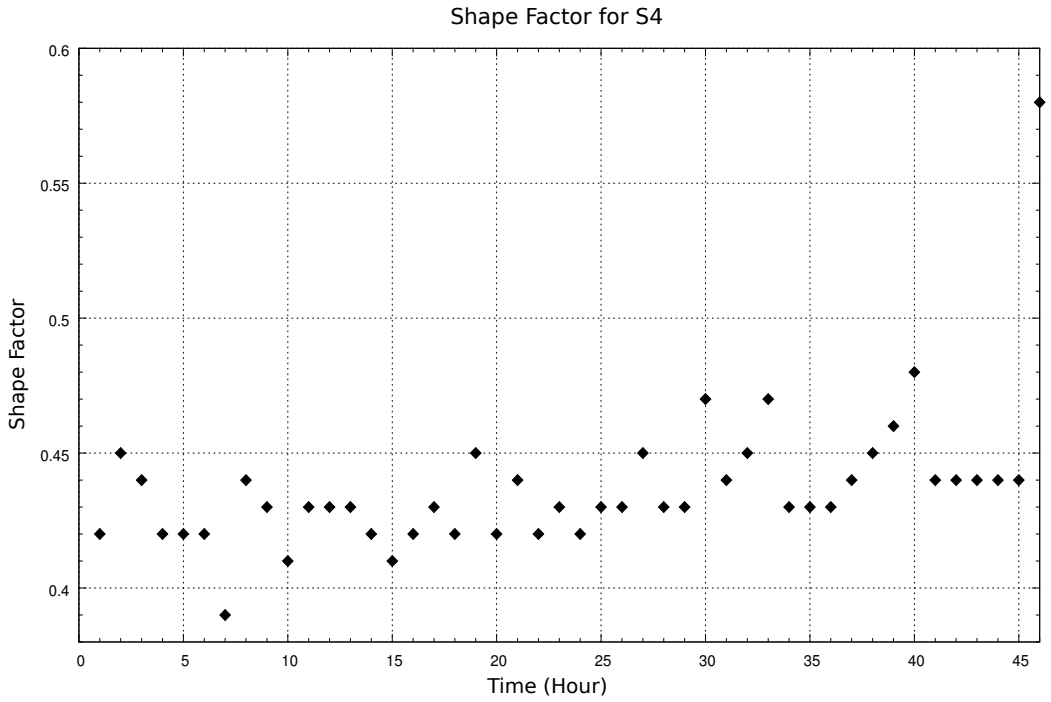

Figure 4.22: There is a slight increase in shape factor values for S4 (eruption), which start closer to 0.42 and end near 0.44. The biggest exception is from the last hour of the swarm which has a very high value of 0.58. The shape factor mean and standard deviation values for S4 are 0.44 and 0.03, respectively.

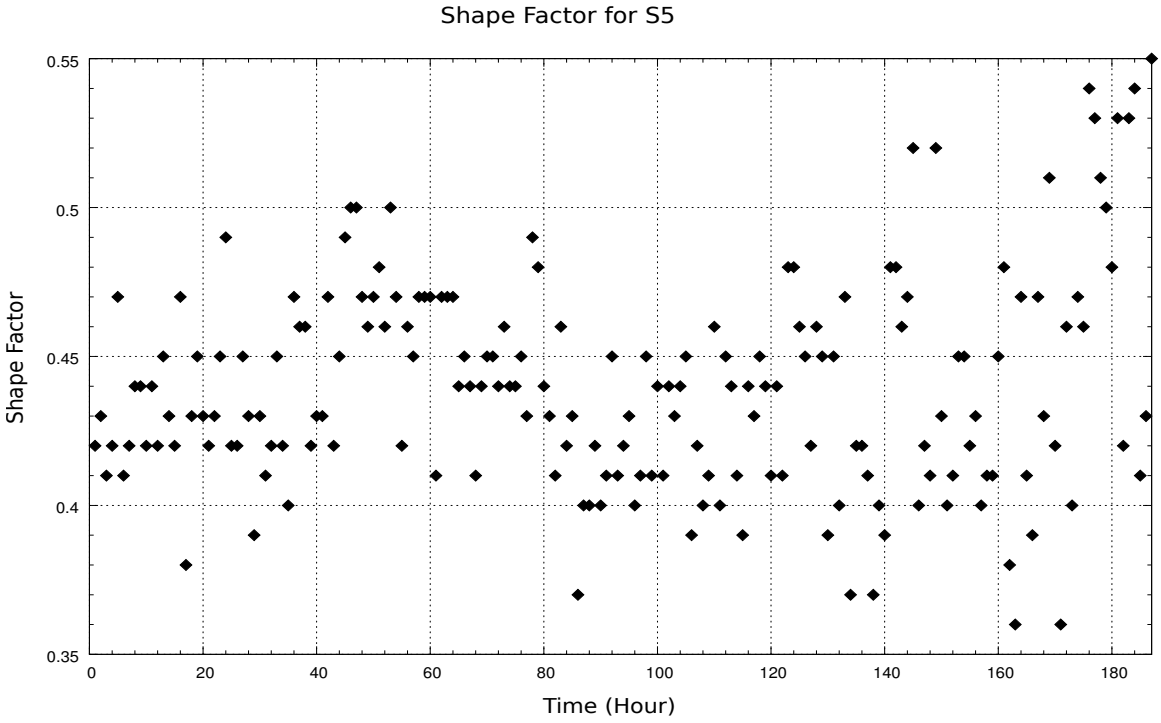

Figure 4.23: Shape factor values for S5 (no eruption) fall between 0.35 and 0.55 with dispersion of values increasing with time into swarm. The shape factor mean and standard deviation values for S5 are 0.44 and 0.03, respectively.

CHAPTER 5:

SUMMARY

As discussed in the previous chapter, there are not many strong correlations between characteristics within earthquake swarms and the outcome of the swarm (eruption or no eruption). The strongest correlation was that swarms that had events with shorter durations resulted in explosions. However, one pattern isn't enough to model which earthquake swarms will lead to eruption. Table 5.1 summarizes the results of all the features for each swarm.

Even though there aren't overall patterns associated with outcomes of earthquake swarms, there are interesting characteristics within each earthquake swarm or within each feature. For example, swarms that had higher duration times tended to have lower time between events. Perhaps the amount of energy in the event determines how often they occur.

There seems to be a characteristic change in the times between events towards the end of the swarms. Both S1 and S2 precede an explosive eruption and the number of events increases before the explosion. This decreases the time between events. S3 and S5 do not precede an eruption and the time between events decreases as the swarm dies off, as would be expected. The exception to this trend is S4. This swarm preceded an explosive eruption, however, and the time between events increases before the eruption.

Also, as expected, central frequency values correlated with the type of earthquake. Specifically, S2 was made up of VT earthquakes and also had the highest central

Swarm	S1	S2	S3	S4	S5
EQ type	Hybrid	VT	Hybrid	LP	LP
Outcome	Eruption	Eruption	No Eruption	Eruption	No Eruption
Duration Mean	7.85	5.61	9.40	8.28	9.87
Duration St. Dev	1.41	1.11	0.86	0.97	0.98
Time Between Mean	50.31	71.36	26.90	27.70	38.17
Time Between St. Dev	32.35	39.57	17.03	12.87	26.32
Central Frequency Mean	4.27	5.26	4.13	4.13	3.94
Central Frequency St. Dev	0.15	0.04	n/a	0.40	0.24
Shape Factor Mean	0.38	0.37	0.44	0.44	0.44
Shape Factor St. Dev	0.01	0.03	n/a	0.04	0.03

Table 5.1: Mean and standard deviation values for each swarm show that the strongest correlation exists between eruption outcome and event duration. There is a slight correlation between eruption outcome and central frequency and shape factor. Time between events show no correlation.

frequency values. S4 and S5 were made up of LP earthquakes and had lower values.

If results from S4 were ignored, there would be a stronger correlation between features and eruption outcome. Values for S1 and S2 (eruption) tended to be similar and values for S3 and S5 (no eruption) were similar. The outlier was usually S4, which preceded an eruption but had values that were more similar to S3 and S5. However, S4 was a significant swarm and cannot be ignored.

5.1 Future Direction

When it comes to searching for patterns within earthquake swarms, it is difficult to cover all possibilities. There are more directions that are left to be studied. These may include earthquake locations, earthquake magnitudes, and other volcanic processes that occur during earthquake swarms.

This study focuses on earthquakes swarms associated with one eruption and the

many explosions that made it up. The next logical step seems to be to compare earthquake swarms that occur with completely failed eruptions versus successful eruptions. It might also be beneficial to compare earthquake swarms from many different volcanoes as opposed to many swarms from one volcano.

It is difficult to say whether or not there are distinct patterns that can better predict volcanic eruptions, but these are a few of the steps that might help answer this problem.

REFERENCES

Allen, RV. 1978. Automatic Earthquake Recognition from Single Traces. *Bulliten of the Seismological Society of America*, **68**(5), 1521–1532.

Bendat, J.S., and Piersol, A.G. 1971. *Random Data: Analysis and Measurement Procedures*. Wiley-Interscience. Chap. Basic Descriptions of Physical Data.

Bull, K., Cameron, C., Coombs, M., Diefenback, A., Lopez, T., McNutt, S., Neal, C., Payne, A., Power, J., Schneider, D., Scott, W., Snedigar, S., Thompson, G., Wallace, K., Waythomas, C., Webley, P., and Werner, C. 2012. *The 2009 eruption of Redoubt Volcano, Alaska*. State of Alaska Department of Natural Resources, Division of Geological and Geophysical Surveys.

Bull, K.F., and Buurman, H. in press. An overview of the 2009 eruption of Redoubt Volcano, Alaska. *Journal of Volcanology and Geothermal Research*.

Chouet, BA. 1996. Long-period volcano seismicity: Its source and use in eruption forecasting. *NATURE*, **380**(6572), 309–316.

Chouet, BA, Page, RA, Stephens, CD, Lahr, JC, and Power, JA. 1994. Precursory swarms of long-period events at Redoubt Volcano (1989-1990), Alaska - their origin and use as a forecasting tool. *Journal of Volcanology and Geothermal Research*, **62**(1-4), 95–135.

Fournelle, J.H., Marsh, B.D., and Myers, J.D. 1994. *The Geology of Alaska*. The Geology of North America, vol. G-1. Geological Society of America. Chap. Age, character, and significance of Aleutian arc volcanism.

Francis, P., and Oppenheimer, C. 2004. *Volcanoes*. Oxford Press.

Hotovec, A.J., Prejean, S.G., Vidale, J.E., and Gomberg, J. in press. Strongly gliding harmonic tremor during the 2009 eruption of Redoubt Volcano. *Journal of Volcanology and Geothermal Research*.

Ketner, D., and Power, J. in press. Characterization of seismic events during the 2009 eruption of Redoubt Volcano, Alaska. *Journal of Volcanology and Geothermal Research*.

Kramer, S.L. 1996. *Geotechnical Earthquake Engineering*. Pearson Education.

Lahr, JC, Chouet, BA, Stephens, CD, Power, JA, and Page, RA. 1994. Earthquake classification, location, and error analysis in a volcanic environment - implications for the magmatic system of the 1989-1990 eruptions at redoubt volcano, alaska. *journal of volcanology and geothermal research*, **62**(1-4), 137–151.

Mazzocchi, M., Hansstein, F., and Ragona, M. 2010. The 2010 Volcanic Ash Cloud and Its Financial Impact on the European Airline Industry. *CESifo Forum*, **11**(2), 92–100.

McNutt, S.R. 1996. *Monitoring and Mitigation of Volcano Hazards*. Springer Berlin Heidelberg. Chap. Seismic Monitoring and Eruption Forecasting of Volcanoes: A Review of the State-of-the-Art and Case Histories.

McNutt, S.R. 2002. *International Handbook of Earthquake and Engineering Seismology*. Academic Press. Chap. 25 Volcano seismology and monitoring for eruptions.

McNutt, SR. 2005. Volcanic seismology. *ANNUAL REVIEW OF EARTH AND PLANETARY SCIENCES*, **33**, 461–491.

Miller, T.P, and Richter, D.H. 1994. *The Geology of Alaska*. The Geology of North America, vol. G-1. Geological Society of America. Chap. Quaternary volcanism in the Alaska Peninsula and Wrangell Mountains, Alaska.

Moran, S.C., Newhall, C., and Roman, D.C. 2011. Failed magmatic eruptions: late-stage cessation of magma ascent. *BULLETIN OF VOLCANOLOGY*, **73**(2), 115–122.

Mulargia, F, Gasperini, P, and Marzocchi, W. 1991. Pattern-Recognition applied to volcanic activity - Identification of the precursory patterns to Etna recent flank eruptions and periods of rest. *Journal of Volcanology and Geothermal Research*, **45**(3-4), 187–196.

Neuberg, J, Luckett, R, Baptie, B, and Olsen, K. 2000. Models of tremor and low-frequency earthquake swarms on Montserrat. *JOURNAL OF VOLCANOLOGY AND GEOTHERMAL RESEARCH*, **101**(1-2), 83–104.

Novelo-Casanova, D. A., and Valdes-Gonzalez, C. 2008. Seismic pattern recognition techniques to predict large eruptions at the Popocatepetl, Mexico, volcano. *JOURNAL OF VOLCANOLOGY AND GEOTHERMAL RESEARCH*, **176**(4), 583–590.

Power, JA, Lahr, JC, Page, RA, Chouet, BA, Stephens, CD, Harlow, DH, Murray, TL, and Davies, JN. 1994. Seismic evolution of the 1989-1990 eruption sequence of Redoubt Volcano, Alaska. *Journal Of Volcanology And Geothermal Research*, **62**(1-4), 69–94.

Power, J.A., Stihler, S.D., Chouet, B.A., Haney, M.M., and Ketner, D.M. in press. Seismic observations of Redoubt Volcano, Alaska - 1989-2010 and a conceptual

model of the Redoubt magmatic system. *Joural of Volcanology and Geothermal Research*.

Scarpetta, S, Giudicepietro, F, Ezin, EC, Petrosino, S, Del Pezzo, E, Martini, M, and Marinaro, A. 2005. Automatic classification of seismic signals at Mt. Vesuvius volcano, Italy, using neural networks. *BULLETIN OF THE SEISMOLOGICAL SOCIETY OF AMERICA*, **95**(1), 185–196.

Schulte-Pelkum, V, Earle, PS, and Vernon, FL. 2004. Strong directivity of ocean-generated seismic noise. *GEOCHEMISTRY GEOPHYSICS GEOSYSTEMS*, **5**(MAR 11).

Stafford, P., Berrill, J., and Pettinga, J. 2009. New predictive equations for Arias intensity from crustal earthquakes in New Zealand. *Journal of Seismology*, **13**, 31–52. 10.1007/s10950-008-9114-2.

Thompson, G., and West, M.E. 2010. Real-time Detection of Earthquake Swarms at Redoubt Volcano, 2009. *SEISMOLOGICAL RESEARCH LETTERS*, **81**(3), 505–513.

Till, A.B., Yount, E., Riehle, J.R., and (U.S.), Geological Survey. 1993. *Redoubt Volcano, Southern Alaska: A Hazard Assessment Based on Eruptive Activity Through 1968*. U.S. Geological Survey bulletin, no. no. 1996. U.S. Department of the Interior, U.S. Geological Survey.

Vallier, T.L., Scholl, D.W., Fisher, M.A., Bruns, T.R., Wilson, F.H., von Huene, R., and Stevenson, A.J. 1994. *The Geology of Alaska*. The Geology of North America,

vol. G-1. Geological Society of America. Chap. Geologic framework of the Aleutian arc, Alaska.

Witham, CS. 2005. Volcanic disasters and incidents: A new database. *JOURNAL OF VOLCANOLOGY AND GEOTHERMAL RESEARCH*, **148**(3-4), 191–233.

APPENDIX A:

APPENDIX

A.1 Automatic Earthquake Picking Algorithm

```
 // K. Carlisle
// catherinecarlisle@u.boisestate.edu

////////////////////////////////////////////////////////////////
// This code will automatically pick seismic events based on the //
// ratio of energy before and after a specific value.           //
////////////////////////////////////////////////////////////////

clear

// 1. Read in seismic data, define variables
oldfile=input('Enter data file name (in quotations).  ');
fp1=file('open',oldfile,'old');
data=read(fp1,-1,2);
file('close',fp1);

s=data(:,2);        //Seismic signal
s=s-mean(s);        //Set mean equal to zero
```

```
t=data(:,1);        //Time in seconds
N=length(t);        //Defines signal length
as=abs(s);       //Use absolute value of signal
dt=t(2,1)-t(1,1);   //Sampling interval

// 2. Input window sizes
wind=400;     //Window size
n=(wind/2);         //Defines middle of window

// 3. Loop st and find energy ratio
for j=wind:N-wind
    x(j)=0;
    for i=(j-n):(j-1) //Half of samples before value j
        x(j)=as(i)+x(j); //Sums amplitudes
    end
    y(j)=0;
    for i=(j+1):(j+n) //Half of samples after value j
        y(j)=as(i)+x(j); //Sums amplitudes
    end
    e(j)=y(j)/x(j); //Energy ratio is the sum of amplitudes after
//divided by the sum of amplitudes after value j.
end
```

```
e=e(st:length(e));   //Changes the length of e to remove 0 values.
e=e-min(e);                  //Sets min value to 0

//4. Plot e, find and plot mean and stdeviation
me=mean(e);
stde=stdev(e);
M=2;              //Constant used in calculating threshold
thresh=(stde*M)+me; //Calculate threshold
eN=length(e);
O=ones(1,eN);
O=O*thresh;     //Creates 1XeN vector of threshold value for plotting
    //purposes

subplot(211)     //Plot signal, energy ratio, and threshold
plot(s)
xtitle('Original Signal, 700 seconds','Sample Number');
subplot(212)
plot(e)
plot(O)
xtitle('Energy Ratio with 3 second window and M=2 threshold'...
  ...,'Sample Number');

// 5. Automatically pick values that exceed predetermined
//threshold.
```

```
n=length(e);
k=1;
while k<n then
if e(k)>thresh then   //If energy ratio is greater than threshold,
        p(k)=k;           //save pick time to new variable (p).
k=k+600;      //Skips ahead 12 seconds to avoid re-picking same
      //event
end
k=k+1;
  end

// 6. Associate picked values with actual times from original
//seismic trace.
tzero=min(t);
ptm(1)=tzero;
for k=2:length(p)
ptm(k)=tzero+(k*dt);
end
i=find(p==0); //Removes zero values
p(i)=[];
ptm(i)=[];

// Save picks in .txt file
newfile=input('Enter name of new file to save picks to');
```

```
fp1=file('open',newfile,'new');
write(fp1,[ptm,p],'(1x,E14.7,2x,E14.7)');
file('close',fp1);
```

A.2 Event Duration from Arias Intensity

```
clear
clf

// K. Carlisle, 3/14/2012

////////////////////////////////////////////////////////
//This program reads in automatic picks for LP events and //
//calculates the events' durations based on the Arias     //
//Intensity.                                              //
////////////////////////////////////////////////////////


//Original Signal
fp1=file('open','hr3nr.txt','old');
a=read(fp1,-1,2);
file('close',fp1);
s=a(:,2);
tm=a(:,1);
```

```
tzero=min(tm);
dt=a(2,1)-a(1,1);
clear a

//Read in autopicks
autopick=input('Enter picks file name  ');
fp1=file('open',autopick,'old');
a=read(fp1,-1,2);
file('close',fp1);
ptm=a(:,1);
ptm=ptm+10;
pick=a(:,2);
pmin=min(ptm);
pmax=max(ptm);
pN=length(pick);

//Solve for duration
for j=1:pN
if pick(j)>0 then
//Create time gate
tmin=ptm(j)-tzero; // Start Time
tmax=tmin+12; //  End Time
if tmax>pmax then
tmax=pmax;
```

```
end
jmin=round(tmin/dt); // Starting Index
jmax=round(tmax/dt); // Ending Index
npts=jmax-jmin+1; // Number of Points between tmin and tmax
  S=s(jmin:jmax); // Signal Window
  TM=tm(jmin:jmax); // Time Window
N=length(S); // Number of points in Window
//Compute Arias Intensity for S
AI(1)=S(1)^2;
for k=2:N
AI(k)=(S(k)^2)+AI(k-1); // Solves Arias Intensity
end
for k=1:N
AI(k)=(AI(k)/AI(N))*100;
end
//Find AI closest to 10%, 90%
[MIN10,I10]=min(abs(AI-5));
[MIN90,I90]=min(abs(AI-95));
//Solve for duration
d(j)=TM(I90,1)-TM(I10,1);
AI=0;
end
end
```

```
//Remove zeros from matrix for when there is no event
i=find(d==0);
d(i)=[];
ptm(i)=[];

//Plot duration
plot2d(ptm,d,-4,rect=[pmin,0,pmax,12]);

//Save duration file
fp2=file('open','dur3Z.txt','new');
write(fp2,[ptm,d],'(1x,E20.10,2x,E20.10)');
file('close',fp2);
```